

RESEARCH ARTICLE | OCTOBER 19 2018

Research Update: Recombination and open-circuit voltage in lead-halide perovskites

Thomas Kirchartz ; Lisa Krückemeier ; Eva L. Unger 



APL Mater. 6, 100702 (2018)

<https://doi.org/10.1063/1.5052164>



Export
Citation

CrossMark

Articles You May Be Interested In


The history of Physics Update

Updating Probabilities

AIP Conference Proceedings (November 2006)

In-situ update of geoparameter databases

J Acoust Soc Am (February 1999)



THE ADVANCED MATERIALS MANUFACTURER®

yttrium iron garnet glassy carbon beamsplitters fused quartz additive manufacturing

zeolites III-IV semiconductors gallium lump copper nanoparticles organometallics

nano ribbons barium fluoride europium phosphors photonics infrared dyes

sapphire windows Nd:YAG cerium oxide polishing powder transparent ceramics CIGS

spintronics raman substrates surface functionalized nanoparticles cermet nanodispersions

silver nanoparticles perovskites MBE grade materials thin film

MOCVD beta-barium borate OLED lighting solar energy

rare earth metals quantum dots sputtering targets fiber optics

osmium scintillation Ce:YAG h-BN deposition slugs

refractory metals laser crystals CVD precursors photovoltaics

anodic aluminum oxide niobate InAs wafers metamaterials borosilicate glass

MOFs AuNPs YBCO superconductors InGaAs

ZnS CdTe indium tin oxide MgF₂ rutile optical glass

perovskite crystals transparent ceramics diamond micropowder

Now Invent.™

www.americanelements.com

© 2001-2023, American Elements is a U.S. Registered Trademark

Research Update: Recombination and open-circuit voltage in lead-halide perovskites

Thomas Kirchartz,^{1,2,a} Lisa Krückemeier,¹ and Eva L. Unger^{3,4}

¹IEK5-Photovoltaik, Forschungszentrum Jülich, 52425 Jülich, Germany

²Faculty of Engineering and CENIDE, University of Duisburg-Essen, Carl-Benz-Str. 199, 47057 Duisburg, Germany

³Chemical Physics and Nano Lund, Lund University, P.O. Box 124, Lund 22100, Sweden

⁴Young Investigator Group Hybrid Materials Formation and Scaling, Helmholtz-Zentrum Berlin GmbH, Kekuléstrasse 5, Berlin 12489, Germany

(Received 14 August 2018; accepted 24 September 2018; published online 19 October 2018)

The high open-circuit voltage and the slow recombination in lead-halide perovskite solar cells has been one of the main contributors to their success as photovoltaic materials. Here, we review the knowledge on recombination in perovskite-based solar cells, compare the situation with silicon solar cells, and introduce the parameters used to describe recombination and open-circuit voltage losses in solar cells. We first discuss the effect of lifetimes and surface recombination velocities on photovoltaic performance before we study the microscopic origin of charge-carrier lifetimes. The lifetimes depend on defect positions and densities and on the kinetic prefactors that control the phonon-assisted interaction between the extended states in the conduction and valence band and the localized defect states. We finally argue that the key to understand the long lifetimes and high open-circuit voltages is a combination of a low density of deep defects and a slow dissipation of energy via multiphonon processes due to the low phonon energies in the lead-halide perovskites. © 2018 Author(s). All article content, except where otherwise noted, is licensed under a Creative Commons Attribution (CC BY) license (<http://creativecommons.org/licenses/by/4.0/>). <https://doi.org/10.1063/1.5052164>

I. INTRODUCTION

Lead-halide perovskites have recently received attention from various scientific communities due to their peculiar optoelectronic properties.^{1–15} In particular, in the case of photovoltaic technologies, efficiency has so far been strongly correlated with the energy, temperature, and cost invested into preparing wafers, films, or devices. For instance, the highest single junction efficiencies are achieved with highly crystalline materials such as epitaxially grown GaAs or monocrystalline silicon wafers.^{16,17} Lower levels of temperature and cost typically result in polycrystalline or amorphous semiconductors such as the different types of thin-film silicon¹⁸ or organic semiconductors that can be used to make solar cells, but those do not achieve efficiencies close to those of monocrystalline semiconductors yet.^{16,19,20} While there have been examples of fairly defect-tolerant polycrystalline semiconductors such as Cu(In,Ga)Se₂^{21–24} during the last decades of solar cell development, the field of solution-processable semiconductors lacked a material that came close to the efficiencies of highly crystalline semiconductors. The fact that lead-halide perovskites have drastically changed this situation^{5,25,26} raises several questions as to why this is the case²⁷ and how one could identify further semiconductors with similar properties.²⁸

Here, we first introduce the necessary terminology to describe recombination in solar cells and then discuss the specific situation of lead-halide perovskites. We discuss lifetimes and recombination coefficients in the bulk and surface recombination velocities describing recombination at interfaces

^aAuthor to whom correspondence should be addressed: t.kirchartz@fz-juelich.de

between the perovskite absorber layer and the electron or hole transport layer. Subsequently, we review the microscopic origins of multiphonon recombination in semiconductors and discuss the implications of this theory for the case of lead-halide perovskites featuring heavy elements like lead and iodine and subsequently low phonon energies. However, there are a range of open questions that are mostly related to surfaces and interfaces and to the topic of anharmonicity: How do we treat surface recombination theoretically and how do we measure surface recombination and what are the implications of the failure of the harmonic approximation in soft semiconductors for the halide perovskites?

A. External vs. internal parameters

Before we start our discussion on recombination in lead-halide perovskites, let us briefly introduce the terminology and the physical parameters that we will use intensively during the discussion. As outlined previously in more detail,^{29,30} we may describe recombination and the losses in open-circuit voltage due to recombination using either external parameters describing the solar cell as a whole or internal parameters that describe what goes on inside the solar cell or solar cell absorber material. The internal parameters (such as mobility, charge carrier lifetime, or internal luminescence quantum efficiency) may vary as a function of position in the volume, while the external parameters (such as open-circuit voltage, fill factor, or external luminescence quantum efficiency) may vary at most as a function of the two-dimensional surface of the solar cell. Whether we describe recombination using external or internal parameters, it is instructive to make the connection between solar cell parameters such as the open-circuit voltage and the luminescent properties of the solar cell or solar cell material.

These luminescent properties are described by the external or internal luminescence quantum efficiency. The external luminescence quantum efficiency,³¹

$$Q_e^{\text{lum}} = \frac{J_{\text{em}}}{J_{\text{rec}}}, \quad (1)$$

is defined as the ratio of recombination currents. Here, J_{em} is the recombination current leading to radiative recombination *and* emission of photons and J_{rec} is the total recombination current. The luminescence quantum efficiency is a crucial component to explain the power conversion efficiency of a light emitting diode.³² However, in addition, Q_e^{lum} is also important to understand photovoltaic power conversion efficiencies via its influence on the open-circuit voltage V_{oc} . Open circuit in an illuminated solar cell is characterized by the situation where photogeneration and recombination currents are exactly balanced because there is no collection current. Just like Q_e^{lum} , the open-circuit voltage is therefore closely connected to the recombination currents. This connection can be expressed mathematically via^{31,33,34}

$$qV_{\text{oc}}^{\text{rad}} - qV_{\text{oc}} = -kT \ln\{Q_e^{\text{lum}}\} > 0, \quad (2)$$

where $V_{\text{oc}}^{\text{rad}}$ is the radiative limit to the open-circuit voltage,³⁵ q is the elementary charge, and kT is the thermal energy. Equation (2) implies that if $Q_e^{\text{lum}} = 1$, the open-circuit voltage is equal to the radiative open-circuit voltage $V_{\text{oc}}^{\text{rad}}$ per definition of the latter. If there is additional non-radiative recombination, the recombination current (radiative and non-radiative) increases for a given voltage and thus the voltage (V_{oc}) at which total recombination and total photogeneration are equal is reduced. For every order of magnitude increase in the recombination current (at a given voltage) relative to the radiative recombination current, Q_e^{lum} will be reduced by one order of magnitude, while the open-circuit voltage will decrease (at room temperature) by $kT \ln\{10\} \approx 60$ meV.

Figure 1(a) illustrates this relation by showing the classical Shockley-Queisser³⁶ (SQ) efficiency vs. band gap plot with a range of data points representing current efficiency records of different photovoltaic (PV) technologies.¹⁶ In addition, Fig. 1(a) shows how the luminescence quantum efficiency Q_e^{lum} reduces the thermodynamic efficiency limits to substantially lower values. While Q_e^{lum} is a strong contribution to efficiencies lower than the SQ limit, there are also other factors limiting efficiency such as incomplete absorption or resistive losses. Thus, it is not possible to directly assign the difference in efficiency between the SQ limit and reality to higher non-radiative losses from Fig. 1(a) alone. However, it is possible to plot the efficiency as a function of the external luminescence quantum

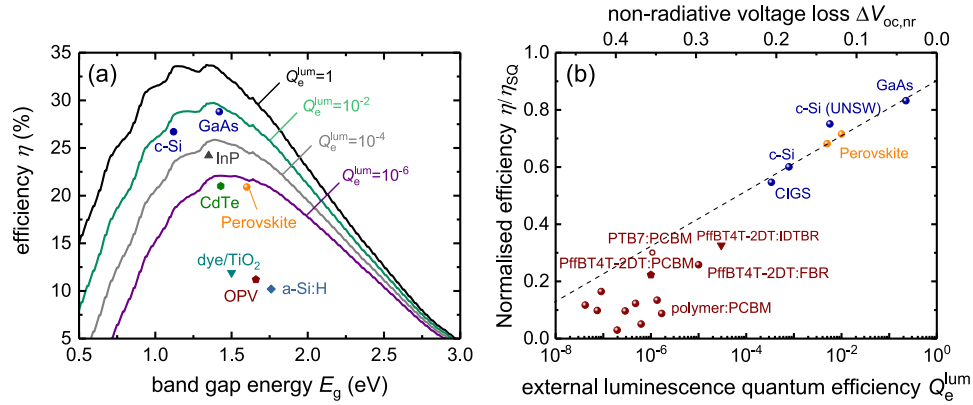


FIG. 1. (a) Efficiency as a function of band gap in the SQ limit and using the external luminescence quantum efficiency as a parameter. In addition, the efficiency of record solar cells using different absorber materials is indicated. (b) Normalized efficiency as a function of external luminescence quantum efficiency or non-radiative voltage loss [linked by Eq. (2)]. Note that the data points in panel (b) are not necessarily record efficiencies because the determination of Q_e^{lum} requires the measurement of an electroluminescence spectrum that is not always available. The dashed line is a guide to the eye.

efficiency Q_e^{lum} for a range of devices where the latter has been either measured experimentally or estimated based on available (photovoltaic) quantum efficiency data.^{35,37} Figure 1(b) shows how the photovoltaic power conversion efficiency η normalized to the value η_{sq} in the SQ limit correlates empirically with Q_e^{lum} . One observation we may derive from Fig. 1(b) is that the most efficient solar cells such as GaAs and crystalline Si have the highest values of Q_e^{lum} with the efficiency advantage of GaAs being mainly related to its advantage in Q_e^{lum} .

In contrast to the external luminescence quantum efficiency, the *internal* luminescence quantum efficiency is defined via

$$Q_i^{\text{lum}} = \frac{R_{\text{rad}}}{R_{\text{tot}}} = \frac{R_{\text{rad}}}{R_{\text{nr}} + R_{\text{rad}}} \quad (3)$$

as the ratio of recombination *rates*. Here, R_{rad} is the radiative recombination rate, R_{nr} is the non-radiative recombination, and R_{tot} is the total recombination rate. One advantage of the internal luminescence quantum efficiency is that it can be related to the properties that are directly measured using transient spectroscopic methods such as lifetimes or recombination coefficients. For instance, the radiative recombination rate is often expressed as

$$R_{\text{rad}} = k_{\text{rad}}np, \quad (4)$$

where k_{rad} is a radiative recombination coefficient in units of cm³/s and n and p are the electron and hole concentrations per volume. Equation (4) assumes that radiative recombination is a bimolecular process proportional to the product of concentrations of free electrons and holes. This assumption is certainly valid in all solar cells where luminescence originates from delocalized band like states that are typically far away from the quasi-Fermi levels at the relatively moderate injection conditions used for photovoltaic operation. However, it is not valid in highly disordered semiconductors (like amorphous Si), where luminescence originates from localized states.^{38–40} If recombination is purely radiative and the device is in high level injection (i.e., $n = p$), the electron concentration would decay with time t after a pulse with $n \sim t^{-1}$ and the photoluminescence intensity ϕ_{PL} would therefore decay as $\phi_{\text{PL}} \sim t^{-2}$.

The non-radiative recombination coefficient, R_{nr} , may also be expressed as a function of electron and/or hole concentration, but the exact relation depends on the recombination mechanism. For instance, if we exclusively consider bulk recombination via a deep defect in a situation where the electron and hole concentrations are equal, we may use an approximate version of the Shockley-Read-Hall (SRH)^{41,42} recombination that gives

$$R_{\text{nr}} = R_{\text{SRH}} = \frac{n}{2\tau_{\text{SRH}}}, \quad (5)$$

where τ_{SRH} is the SRH lifetime assumed identical for electrons and holes. The significance of Eq. (5) is that such a model is often used to fit exponential decays in transient measurements such as transient photoluminescence. If non-radiative recombination controls the decay of charge carriers and the device is in high level injection ($n = p$), the decay would be $n \sim \exp(-t/(2\tau_{\text{SRH}}))$ and the decay of the photoluminescence flux would be $\phi_{\text{PL}} \sim \exp(-t/\tau_{\text{SRH}})$. Note that the decay of photoluminescence caused by radiative recombination may be exponential due to non-radiative recombination controlling the decay of charge carriers. This is not in contrast to the statement that radiative recombination itself is bimolecular. Thus, the lifetime of a sample measured by transient photoluminescence is by no means a “radiative” lifetime if non-radiative recombination dominates even though the measurement principle is based on the detection of emission caused by radiative recombination.

While we have learned how to relate the external luminescence quantum efficiency Q_e^{lum} to the open-circuit voltage V_{oc} and the internal luminescence quantum efficiency Q_i^{lum} to experimentally observable quantities like charge carrier lifetimes, τ , and recombination coefficients, k , we have not yet discussed a connection between the internal and external quantities. If we imagine radiative recombination to happen within the bulk of our solar cell absorber material, the photon created by that recombination event may either contribute to the externally measured luminescence that defines J_{em} or be reabsorbed within the device. The photon has a probability p_e of coupling out of the solar cell in which case it can be detected. It also has a probability p_r of being reabsorbed by the absorber layer itself in which case it will make additional electron-hole pairs that may cause additional radiative recombination. This process is referred to as photon recycling.

The photon may also be reabsorbed in some of the contact layers like the metal back reflector that will not lead to additional radiative recombination events. If we call this quantity the probability p_a of parasitic absorption, we know that $p_e + p_a + p_r = 1$ must hold. If we ignore all spatial dependences of the recombination rates, the relations connecting the rates with the recombination currents become rather simple. For instance, we can write $J_{\text{em}} = qdp_e R_{\text{rad}}$, where d is the thickness of the absorber layer or $J_{\text{rec}} = qd[R_{\text{SRH}} + (1 - p_r)R_{\text{rad}}]$, where we have accounted for probability p_r for photon recycling which essentially reduces the effective radiative recombination rate.

In the spirit of this approximation of ignoring all spatial dependences of the recombination rates, we obtain fairly simple relations between the external and internal luminescence quantum efficiency reading^{30,43}

$$Q_e^{\text{lum}} = \frac{J_{\text{em}}}{J_{\text{rec}}} = \frac{p_e R_{\text{rad}}}{R_{\text{nrad}} + (1 - p_r)R_{\text{rad}}} = \frac{p_e Q_i^{\text{lum}}}{1 - p_r Q_i^{\text{lum}}} = \frac{p_e Q_i^{\text{lum}}}{(1 - Q_i^{\text{lum}}) + (p_e + p_a)Q_i^{\text{lum}}}. \quad (6)$$

Equation (6) allows us in consequence to rewrite Eq. (2) in terms of the internal luminescence quantum efficiency. Thus, we may express the open-circuit voltage as a function of the internal luminescence quantum efficiency as

$$qV_{\text{oc}} = qV_{\text{oc}}^{\text{rad}} + kT \ln \left\{ \frac{p_e Q_i^{\text{lum}}}{1 - p_r Q_i^{\text{lum}}} \right\}. \quad (7)$$

We have now introduced recombination currents, recombination rates, and charge carrier lifetimes and discussed how they relate to the open-circuit voltage. Equation (7) illustrates how the relation between internal material properties and external properties of devices such as the V_{oc} become more complicated as the probabilities of photon outcoupling and reabsorption need to be taken into account. The above equations are—within the logic of their approximations—quite generic and are valid and useful for any photovoltaic technology. In the following, we will use this terminology and apply it to the case of lead-halide perovskite based solar cells.

B. Importance of non-radiative recombination

In this section, we first start introducing internal parameters and motivate why we think that the topic of recombination and therefore the charge-carrier lifetime in lead-halide perovskites deserves special attention. For a random photovoltaic technology, one may identify three key material parameters that determine and potentially limit the efficiency of photovoltaic absorber materials. These are the absorption coefficient, α , the charge-carrier lifetime, τ , and the mobility, μ . In the following, we

will argue why in the situation of a highly absorbing material like most lead-halide perovskites, the lifetime is of particular importance.

Highly absorbing materials require low thicknesses to absorb most of the solar spectrum ϕ_{sun} above the material's band gap. Here, ϕ_{sun} is the AM1.5G solar spectrum per area, time, and energy interval, which is usually tabulated⁴⁴ as a function of photon energy E or wavelength. The relation between absorbed photons and thickness can be quantitatively expressed by plotting the short-circuit current density

$$J_{\text{sc}} = q \int_0^{\infty} a(E) \phi_{\text{sun}}(E) dE \quad (8)$$

as a function of thickness. In order to do this, we need to agree on an optical model that connects the internal property (the absorption coefficient α) to an external property (the absorptance a). If we use for the moment a simple Lambert-Beer model with a perfect back reflector and zero reflection at the front, we obtain $a = 1 - \exp(-2\alpha d)$. Using the absorption coefficient of $\text{CH}_3\text{NH}_3\text{PbI}_3$ (MAPI) taken from Ref. 45, we may then plot J_{sc} as a function of the absorber thickness d as represented by the dashed line Fig. 2(a). While in the high-mobility limit, J_{sc} is monotonously increasing with thickness, the open-circuit voltage will typically decrease.^{30,46,47}

Here we calculate the open-circuit voltage as the voltage where the recombination current due to radiative and non-radiative SRH recombination is equal to J_{sc} given by Eq. (8). The exact dependence of the open-circuit voltage on thickness depends on the type of recombination (radiative or non-radiative, bulk or surface)⁴⁸ but for the relevant situation of combining radiative and non-radiative bulk recombination with perfect surfaces (no surface recombination), V_{oc} will decrease monotonously. This is due to the case that in this limit of high mobilities, the recombination current increases

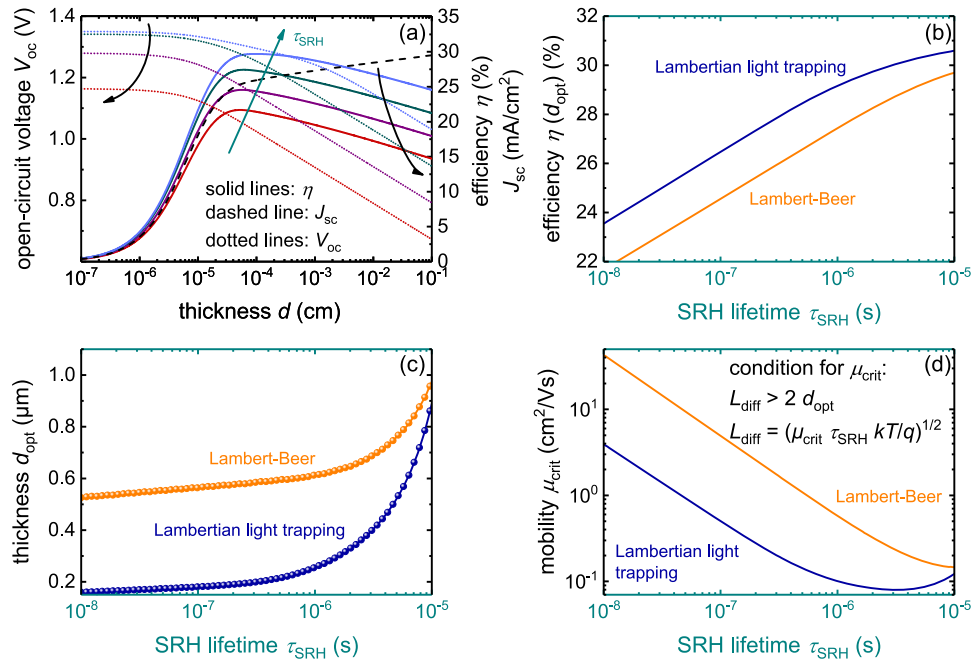


FIG. 2. (a) Efficiency η (solid lines), short-circuit current density J_{sc} (dashed line), and open-circuit voltage V_{oc} (dotted lines) as a function of thickness in the limit of infinite mobilities, perfect surfaces, and a simple Lambert-Beer like absorption model with a perfect back reflector. The parameter used is the value of the SRH lifetime $\tau_{\text{SRH}} = 10 \text{ ns}$, 100 ns , $1 \mu\text{s}$, and $10 \mu\text{s}$. We observe that the efficiency always has a maximum at a finite thickness. (b) Efficiency at the optimum thickness as a function of τ_{SRH} for two optical models, namely, the Lambert-Beer model used in (a) as well as with Lambertian light trapping. (c) shows the corresponding optimum thickness for the two cases. (d) From the condition that the diffusion length should be at least twice the optimum thickness, we obtain a critical mobility for the two cases that allows good charge extraction for a layer with the thickness d_{opt} even for zero electric field.

linearly with thickness, while the short-circuit current saturates at thicknesses where nearly complete absorption above the band gap is achieved. Using a simple model for the recombination currents as described in detail in paragraph 5.2 in Ref. 49, we calculate V_{oc} for a range of different non-radiative lifetimes τ_{SRH} . Given the opposing trends of J_{sc} and V_{oc} with thickness, it is clear that the efficiency in the limit of high mobilities and in the presence of non-radiative bulk recombination must also have a maximum at a finite thickness.²⁹ Figure 2(a) shows this maximum and how it increases with the SRH lifetime. Figure 2(b) shows how the efficiency at the optimum thickness depends on the SRH lifetime for two different optical models. The lower line corresponds to the data in Fig. 2(a) and shows the more pessimistic optical model without any light scattering, while the upper line shows the situation of Lambertian light trapping described in Ref. 50 and used in several publications dealing with realistic efficiency limits.^{47,51,52} Figure 2(c) shows the optimum thickness d_{opt} for the two optical models. For the case without light trapping, d_{opt} is in the range of 500–600 nm for realistic lifetimes below 1 μs . Toward higher lifetimes, the optimum thickness increases quickly and will approach infinity for the situation of radiative recombination only.⁴⁹ So far, these simulations illustrate that the absorption coefficient is high enough to ensure that already thicknesses below 1 μm will give optimum efficiencies if realistic values for the charge-carrier lifetime are assumed. This allows us to estimate the mobilities needed to achieve efficient collection. Collection may be aided by electric fields,⁵³ but as long as there are no barriers impeding the extraction of majority carriers, collection by diffusion would allow us to obtain a lower limit to the collection efficiency of charge carriers for a given thickness and mobility-lifetime product. If we assume that the diffusion length should be at least twice the optimum thickness given in Fig. 2(c), we obtain—for both optical models—a condition for the critical mobility needed to achieve collection in a field free absorber layer of thickness d_{opt} and charge carrier lifetime τ_{SRH} . This critical mobility is presented in Fig. 2(d). If we compare the results with experimental data on MAPI and related lead-halide perovskites, we see that lifetimes are typically in the range of 100 ns–1 μs ^{45,54–59} with some exceptions⁶⁰ approaching several μs . Reported mobilities vary over a large range but are generally higher than 1 cm^2/Vs and not usually much higher than 100 cm^2/Vs in thin films.⁶¹ This suggests that mobilities are lower⁶² than in other semiconductors used for photovoltaics such as GaAs and crystalline Si, but they are sufficiently high to enable efficient charge carrier collection as long as the lifetimes are indeed longer than 100 ns.

These considerations lead us and many authors before us^{5,26,63} to conclude that indeed the long charge-carrier lifetimes or in other words the low rates of non-radiative recombination at a given density of charge carriers are a highly remarkable and relevant property of lead-halide perovskites that therefore demands further investigation and discussion. Here we want to therefore review what is known about the importance of non-radiative recombination in solar cells in general and perovskite-based solar cells in particular and then focus on the origin of the lifetimes, i.e., the defect densities, the origin of defects, and possible explanations for the capture coefficients of these defects.

C. Why slow radiative recombination is less important

As we have seen before, measuring radiative recombination at a certain injection current (i.e., with a fixed amount of total recombination) is a useful way to characterize and quantify non-radiative recombination via Eq. (1) and its impact on V_{oc} via Eq. (2). However, unlike sometimes stated in the literature,⁶⁴ photovoltaic performance is rarely affected by high or low coefficients of radiative recombination. This is due to the fact that radiative recombination coefficients k_{rad} are linked to absorption coefficients α via the principle of detailed balance.⁶⁵ In the specific case of detailed balance between absorption and emission,⁶⁶ we may write

$$k_{rad}n_i^2 = \int_0^\infty 4\alpha n_r^2 \phi_{bb} dE, \quad (9)$$

where n_r is the refractive index and n_i is the intrinsic carrier concentration. The left-hand side of Eq. (9) represents radiative recombination in thermal equilibrium, while the right-hand side represents absorption of photons in thermal equilibrium. Here, the black body spectrum ϕ_{bb} at the temperature T of the solar cell is given as

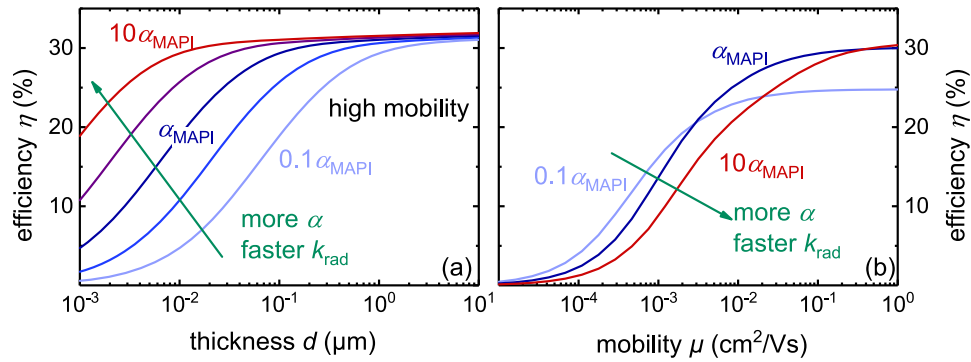


FIG. 3. (a) Radiative efficiencies as a function of thickness for high mobilities for different values of k_{rad} and α always obeying Eq. (9). Note that for lower thicknesses, fast radiative recombination would outperform slow radiative recombination. (b) Efficiency as a function of mobility in the radiative limit. The active layer thickness is held constant here at $d = 300$ nm.

$$\phi_{\text{bb}}(E) = \frac{2\pi E^2}{h^3 c^2} \frac{1}{[\exp(E/kT) - 1]} \approx \frac{2\pi E^2}{h^3 c^2} \exp\left(\frac{-E}{kT}\right), \quad (10)$$

with h being Planck's constant and c being the speed of light in vacuum. Thermal radiation at room temperature is mainly in the far infrared; however, the very broad black body spectrum defined by Eq. (10) has a tail of high energy photons that are absorbed and lead to photogeneration of charge carriers in the semiconductor and makes the r.h.s of Eq. (9) nonzero.

Figure 3(a) shows efficiencies in the high mobility limit as a function of thickness for different values of k_{rad} and α always obeying Eq. (9). The simulations were performed as described in Ref. 47 with the parameters (other than k_{rad} and α) being given in Table I, with the doping density being zero. In addition, non-radiative recombination in the bulk and at surfaces was omitted to show the influence of radiative recombination only. For high thicknesses, the efficiency would always be the same, while for lower thicknesses, the devices with fast radiative recombination would actually outperform the ones with slower radiative recombination. This is due to the fact that higher absorption at the price of faster recombination is more beneficial for lower thicknesses than less efficient absorption and slower recombination. Any beneficial effects of small k_{rad} values are only apparent when mobilities are reduced. Figure 3(b) shows that if efficiency is plotted as a function of mobility but with constant thickness (of 300 nm), the cells with smaller k_{rad} values outperform the ones with higher k_{rad} values only for very low mobilities. Thus, reducing radiative recombination implies reducing absorption which is typically not beneficial for a solar cell. The exception is the case of extremely low mobilities. Solar cell materials dominated by radiative recombination with mobilities low enough to run into a mobility limitation as shown in Fig. 3(b) are so far unknown. Organic semiconductors may be close to the radiative limit and have low mobilities, but because organic semiconductors for solar cells are usually used in a donor-acceptor blend system, the absorber combinations relevant for photovoltaics are far from the radiative limit, as shown in Fig. 1(b) and a variety of publications.^{37,67–69}

TABLE I. Parameters used for the simulations if not noted otherwise.

Parameter	Value
Radiative recombination coefficient k_{rad}	$8 \times 10^{-10} \text{ cm}^3/\text{s}$
Lifetime τ_{SRH}	500 ns
Mobility $\mu_n = \mu_p$	$10 \text{ cm}^2/\text{Vs}$
Effective density of states N_C (conduction band)	$2.2 \times 10^{18} \text{ cm}^{-3}$
N_V (valence band)	$2.2 \times 10^{18} \text{ cm}^{-3}$
Surface recombination velocity	Variable (see text)
Doping concentration	0 or 10^{15} cm^{-3} (see text)
Dielectric permittivity ϵ_r	33.5
Thickness	300 nm

II. FROM CHARGE-CARRIER LIFETIMES TO SOLAR CELL EFFICIENCIES

Section I A introduced the internal parameters such as lifetimes, recombination coefficients, and internal luminescence quantum efficiencies and external parameters such as external luminescence quantum efficiency and open-circuit voltage. Section I A also introduced the equations we need to relate these quantities to each other. In the following, we want to illustrate these relations using material parameters that have been determined for MAPI films in the literature and thereby discuss the relative importance of different recombination mechanisms.

A. Different recombination mechanisms

Figure 4 shows how one can estimate the importance of different recombination mechanisms by going from the situation of a film on glass with (hypothetically) non-recombination active surfaces

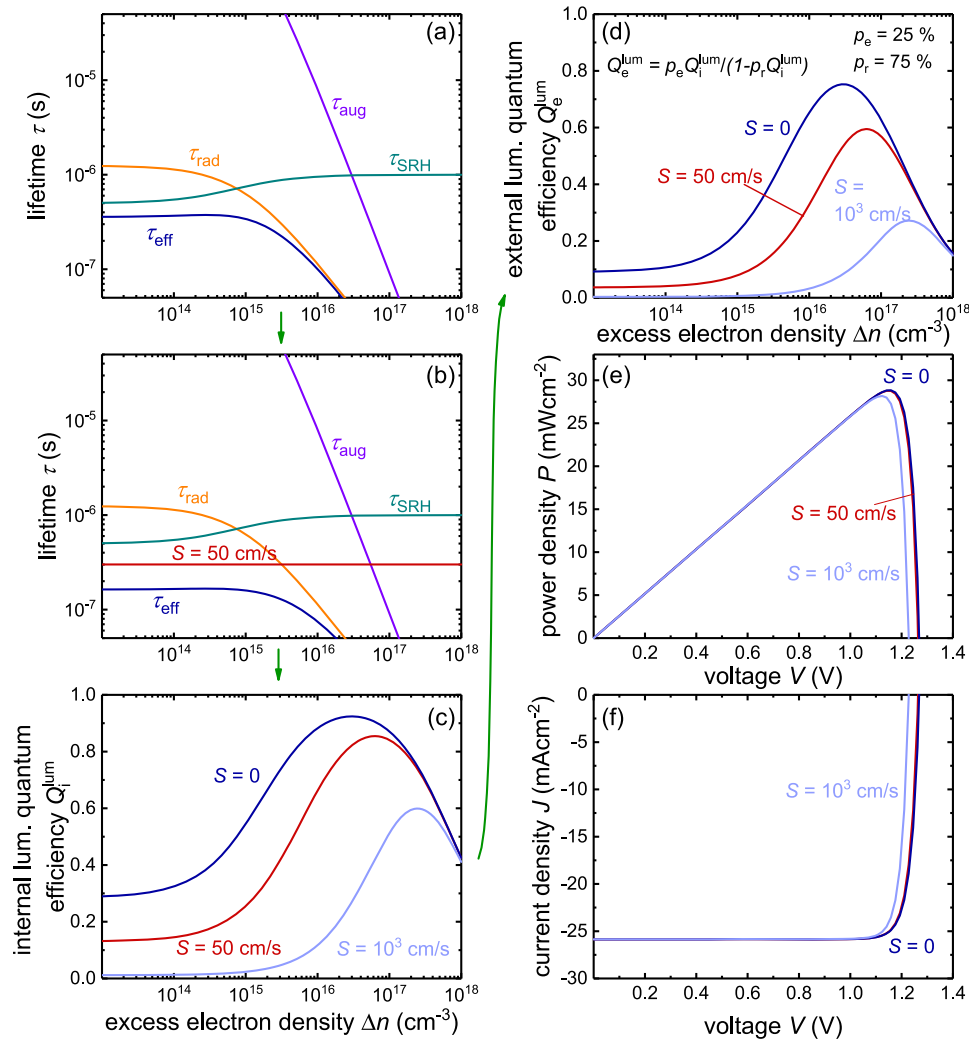


FIG. 4. **From effective lifetimes to efficiencies:** (a) Effective lifetime as a function of excess electron density for different bulk recombination mechanisms neglecting surface recombination. The Auger coefficient is $C = 5.4 \times 10^{-28}$ cm⁶/s, and the coefficient for radiative recombination is $k_{\text{rad}} = 8 \times 10^{-10}$ cm³/s from Ref. 45, while we assume a SRH lifetime of 500 ns and doping density $N_A = 10^{15}$ cm⁻³. (b) The same but now including surface recombination with a surface recombination velocity $S = 50$ cm/s on both surfaces of the film. (c) The resulting internal luminescence quantum efficiency for three different surface recombination velocities $S = 0, 50$, and 10^3 cm/s. Assuming that we now make an idealized solar cell with Q_i^{lum} as given in (c), panel (d) shows the external luminescence quantum efficiencies Q_e^{lum} assuming $p_e = 25\%$ for a system with Lambertian light trapping.⁴⁷ Finally, panels (e) and (f) show the power density and current density-voltage curves for a solar cell including the effect of photon recycling. All panels assume a 300 nm thick MAPI film with the optical data as given in Ref. 45.

to a situation that includes recombination at surfaces. Subsequently, we include the optical effects of outcoupling and photon-recycling and then move toward external quantities such as the power conversion efficiency. Figure 4(a) shows the bulk lifetimes τ as a function of excess electron density Δn . This type of plot is not common in the literature on lead-halide perovskites, but it is the standard way of discussing lifetimes of crystalline Si wafers. It allows us to better observe the differences between different recombination mechanisms. In order to illustrate the difference between high and low level injection—i.e., between the situation where photogenerated charge carriers are present in excess of the concentration of charges in the dark (high level injection) or vice versa (low level injection)—the perovskite layer is assumed to be doped p-type with a doping density $N_A = 10^{15} \text{ cm}^{-3}$. Note that both the doping type and density are chosen relatively arbitrarily. We define the lifetime for any given process always via $\tau_i = \Delta n / R_i$, where R_i is the recombination rate of a certain process (e.g., $i = \text{“Aug”}$ for Auger, “rad” for radiative, or “SRH” for Shockley-Read-Hall recombination). Figure 4(a) includes three recombination mechanisms, namely, Auger recombination with a rate given by $R_{\text{aug}} = C(n^2p + p^2n)$ with the Auger coefficient $C = 5.4 \times 10^{-28} \text{ cm}^6/\text{s}$ being taken from Ref. 70. Radiative recombination is a bimolecular process with a rate being given by Eqs. (4) and (9). Values for the radiative recombination coefficient k_{rad} in the literature range from 7×10^{-11} to $\sim 9 \times 10^{-10} \text{ cm}^3/\text{s}$.⁷¹ Here, we use a value $k_{\text{rad}} = 8 \times 10^{-10} \text{ cm}^3/\text{s}$ which is compatible with the absorption coefficient used and with the van Roosbroek-Shockley equation [see Eq. (9)]. Finally, we show the lifetime resulting from SRH recombination via a deep defect. The rate for a deep defect is given by

$$R_{\text{SRH}} = \frac{np - n_0p_0}{n\tau_p + p\tau_n}, \quad (11)$$

where $\tau_{n/p} = (k_{n/p}N_T)^{-1}$ are the electron and hole lifetimes, and n_0 and p_0 are the equilibrium concentrations of electrons and holes, respectively. Here $k_{n/p}$ is the electron and hole capture coefficient (unit is cm^3/s , i.e., same as k_{rad}), while N_T is the trap density. The values for k_n and k_p are expected to vary over orders of magnitude depending on the position of the defect as discussed later in Sec. III C. However, for the purpose of illustrating the general idea in Fig. 4, we choose $\tau_n = \tau_p = \tau_{\text{SRH}} = 500 \text{ ns}$ which is a typical value for the lifetime obtained from transient photoluminescence measurements of MAPI films on glass.⁴⁵ In addition to the lifetimes for Auger, radiative, and SRH recombination, Fig. 4(a) also shows the effective lifetime τ_{eff} resulting from the combination of all three processes. Because recombination rates add up, we need to calculate the inverse of sum of the inverse lifetimes for every individual process, i.e., $\tau_{\text{eff}} = (\tau_{\text{rad}}^{-1} + \tau_{\text{aug}}^{-1} + \tau_{\text{SRH}}^{-1})^{-1}$.

While Fig. 4(a) only includes bulk recombination mechanisms, in reality recombination at surfaces is an important factor that may be limiting efficiency in finished solar cells.⁷² Therefore, Fig. 4(b) includes the effect of surface recombination in the same type of figure. In order to relate the effect of surface recombination to that of bulk recombination, we need to define a surface recombination lifetime τ_s which contains the effects of diffusion to the surface and recombination at the surface. For the case of surface recombination velocities S for minority carriers being equal for both surfaces and for the case of low level injection, the surface lifetime

$$\tau_s = \frac{d}{2S} + \frac{d^2}{D\pi^2}, \quad (12)$$

where d is the thickness of the absorber and D is the diffusion constant of the minority carriers that is related to the mobility μ via the Einstein relation ($D = \mu kT/q$). The first term on the r.h.s. corresponds to the recombination process at the surface, while the second term takes into account diffusion to the surface. Thus, even if surface recombination was infinitely fast ($S \rightarrow \infty$), the surface lifetime τ_s would be nonzero taking into account that diffusion to the surface takes time and slows down the whole process. One obvious problem with Eq. (12) is that it is derived by solving the time-dependent diffusion equation in one dimension for one type of charge carrier (e.g., electrons in a p-type semiconductor). Thus, deviations from this equation are possible in high level injection. Because we are not aware of a version of Eq. (12) valid for high level injection as well, we use a constant low level injection surface lifetime for Fig. 4(b) based on Eq. (12) and an arbitrary surface recombination velocity $S = 50 \text{ cm/s}$ just for the purpose of illustration. While $S = 50 \text{ cm/s}$ is a fairly

low value for the standards of, e.g., passivation layers on crystalline Si, the surface recombination further reduces the effective lifetime relative to panel (a).

Figure 4(c) illustrates the translation of lifetimes into the internal luminescence quantum efficiency $Q_i^{\text{lum}} = \tau_{\text{eff}}/\tau_{\text{rad}}$. In order to show how the influence of the surfaces affects the internal luminescence quantum efficiency, we plot $S = 0$ [compatible with panel (a)], $S = 50$ cm/s [compatible with panel (b)], and $S = 10^3$ cm/s.

Figure 4(d) adds outcoupling and photon recycling to the discussion and illustrates how Q_i^{lum} translates into an external luminescence quantum efficiency Q_e^{lum} . We chose an outcoupling efficiency of 25% (corresponds to a MAPI thickness of 300 nm, Lambertian light trapping, and outcoupling only from one surface with the other being perfectly reflective⁴⁷) and a reabsorption probability $p_r = 0.75$, implying that parasitic absorption is neglected.

When comparing the calculated values for Q_e^{lum} with experimental data from the literature, it is important to consider the carrier density under which the measurement is taken. This can be clearly seen from the strong dependence of Q_e^{lum} on Δn shown in Fig. 4(d). The highest values of Q_e^{lum} at a charge carrier density comparable to one sun at open circuit so far are 0.5% reported by Bi *et al.*⁵⁶ for a double cation and double halide perovskite solar cell and ~1% for a quadruple cation, double halide perovskite reported by Saliba *et al.*²⁵ The Q_e^{lum} of this cell goes up to 3.8% at forward voltages of 2 V. Substantially higher values (~37%) have only been reported for MAPI films on glass covered with (non-conducting) passivation layers.⁷⁰ This finding further supports the importance of investigating recombination at interfaces between perovskite absorber layers and selective contact layers, where the term “selective” means that injection and extraction of majority carriers is as efficient as possible, while recombination of minority carriers is as inefficient as possible.

Finally, Figs. 4(e) and 4(f) illustrate the situation where the material properties discussed so far and the optical properties (outcoupling and reabsorption) are included in a full device simulation. Panel (e) shows the power-density voltage relation zoomed in to the maximum power point, while panel (f) shows the current-voltage curves in the fourth quadrant. We observe that $S = 50$ cm/s has fairly little influence on efficiency, while $S = 1000$ cm/s already leads to substantial losses in efficiency that are caused mostly by a loss in open-circuit voltage.

B. Comparing MAPI with crystalline Si

In order to put the lifetimes and internal luminescence quantum efficiencies presented earlier into perspective, we compare the values with crystalline Si, still the by far most important semiconductor for industrial photovoltaics. To reduce the complexity of the graphs, we ignore bulk recombination via defects for Si and for MAPI and concentrate only on the intrinsic bulk recombination mechanisms (Auger and radiative) and on the surfaces which may limit or at least affect current efficiencies and V_{oc} s in both technologies. Figure 5(a) shows the effective lifetime τ_{eff} , the Auger lifetime τ_{aug} , and radiative lifetime τ_{rad} of a Si wafer with an acceptor density $N_A = 10^{16}$ cm⁻³. In addition, we assume surface recombination to happen with a surface recombination velocity S ranging from $S = 1$ cm/s to 100 cm/s. The diffusion constant for electrons in p-type Si is taken to be 27 cm²/s corresponding to a typical electron mobility slightly above 1000 cm²/Vs.⁷³

Figure 5(b) shows in comparison the effective lifetime of MAPI. We observe that radiative recombination is of only minor relevance for Si because Auger recombination limits the effective lifetime^{74,75} in the bulk of a floatzone wafer where the defect density is low enough to suppress defect related recombination in the bulk (but not at the surface). In lead-halide perovskites, Auger recombination is irrelevant for non-concentrated sunlight because radiative recombination dominates at high charge-carrier densities. In both devices, surface recombination matters and may effectively reduce the lifetime.

Figures 5(c) and 5(d) show the resulting internal luminescence quantum efficiencies that result from the lifetimes shown in panels (a) and (b). The important fact to note here is that while Si has the much longer effective lifetimes for a given value of S , it actually has lower internal luminescence quantum efficiencies. This means that even though Si might always have much better lifetimes and diffusion lengths than MAPI (due to a combination of low radiative recombination coefficients and low defect densities), MAPI may still come closer to the radiative efficiency limit than Si because it does not suffer from Auger recombination and exhibits relatively long lifetimes. The efficiency

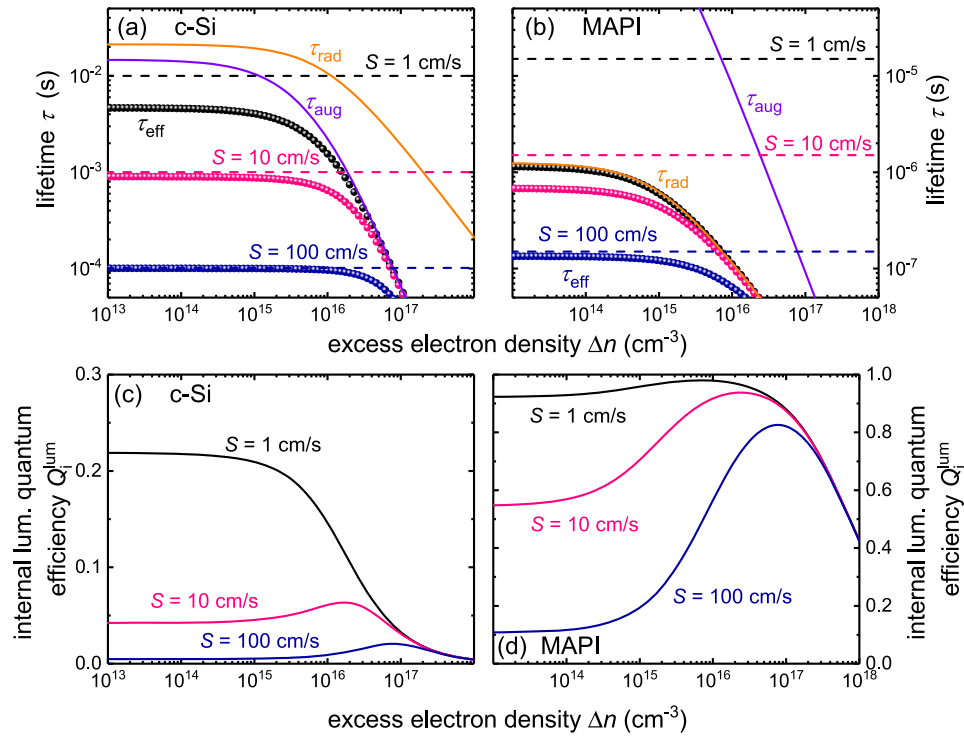


FIG. 5. (a) Radiative and Auger lifetime (τ_{rad} and τ_{aug}) of crystalline Si (200 μm thick p-type wafer with a doping density $N_A = 10^{16} \text{ cm}^{-3}$). In addition, the effective lifetime (symbols) is drawn for three different surface recombination velocities $S = 1, 10$, and 100 cm/s . (b) Radiative and Auger lifetime of MAPI (300 nm thick film with an assumed doping density $N_A = 10^{15} \text{ cm}^{-3}$) and the effective lifetime (symbols) for three different surface recombination velocities $S = 1, 10$, and 100 cm/s . For (a) and (b), the surface lifetimes are drawn with dashed lines. (c) and (d) show the corresponding internal luminescence quantum efficiencies for the three surface recombination lifetimes. Note that the lifetimes are generally higher for c-Si, but the internal luminescence quantum efficiencies are higher in the case of MAPI due to the much shorter radiative lifetime. Note the different scales of the y-axes.

targets for single junction cells made from lead-halide perovskites with band gaps $\sim 1.6 \text{ eV}$ and from Si are therefore similar. The Auger limit^{74,76,77} restricts the efficiencies of Si to about 29% (26.6% already achieved), while the Shockley-Queisser limit restricts the efficiency of a solar cell with a band gap $\sim 1.6 \text{ eV}$ (MAPI) to $\sim 30\%$ (compared to $\sim 33\%$ for Si and GaAs). A more detailed discussion of this topic has recently been published by Pazos-Outon *et al.*⁷⁸

C. Recombination in devices

Figure 4 already includes the transition from material and interface properties like τ and S to the properties of a device. This section now provides a closer look at the relation between lifetime and surface recombination velocity and the device performance of a MAPI based solar cell. Again we need to assume an optical model to relate internal to external properties as discussed in more detail in Refs. 29 and 47. This is important for various reasons: We need to be able to calculate the photocurrent and the radiative recombination current based on the absorptance of a semiconductor. This requires a way of relating the absorption coefficient, thickness, and refractive index to the absorptance. In addition, if we simulate the efficiency of a system with finite mobilities close to the radiative limit, we need to consider reabsorption effects, i.e., photon recycling. For instance, Eq. (6) relates internal and external luminescence quantum efficiencies to each other ($Q_e^{\text{lum}} = p_e Q_i^{\text{lum}} / (1 - p_r Q_i^{\text{lum}})$). The denominator of this equation decreases below 1 if $p_r Q_i^{\text{lum}}$ is sufficiently high. Thus, if we have reabsorption happening with a high probability p_r and if the reabsorbed photons create electron-hole pairs that recombine radiatively with a sufficiently high probability Q_i^{lum} , photon recycling starts contributing substantially to the value of Q_e^{lum} that then enters Eq. (7) and leads to an increase in V_{oc} . The model used for Eq. (6)

assumes that parameters like Q_i^{lum} and p_r are constant as a function of position. However, this is not necessarily the case. This spatial dependence can be most easily understood in the case of surface recombination. Surface recombination leads to a decrease in the charge-carrier concentration toward the surfaces and therefore to a reduced quasi-Fermi level splitting and a reduced luminescence close to the interfaces of the device. Thus, using Eq. (6) can only be an approximation. In order to include spatial dependences of Q_i^{lum} and the effect of photon recycling, we have to use an optical model that calculates how radiative recombination at any position in the absorber leads to reabsorption in any other position of the same absorber. A numerical implementation of these radiative interactions has been developed by Mattheis⁷⁹ for two representative cases, Lambert-Beer type absorption and Lambertian light trapping (i.e., the front surface randomizes the direction of light by some unspecified means of light scattering). Here we use the Lambertian light trapping case as an example. It generally provides higher efficiencies but lower open-circuit voltages for a given thickness as compared to the Lambert-Beer case. A comparison between the different optical models can be found in Ref. 47.

Figures 6(a) and 6(b) show the simulated (a) efficiency and (b) open-circuit voltage as a function of the bulk lifetime including and excluding the effect of photon recycling. Excluding photon recycling means here that we numerically omit the internal generation rate that is due to photons generated inside the absorber. This is mathematically the same as assuming that all bimolecular recombination is non-radiative; however, it has to be clear that the absence of photon recycling is an unphysical scenario because of the impossibility of avoiding radiative recombination and reabsorption. The purpose of showing the curve without photon recycling is to illustrate the magnitude of the effect. This comparison is relevant for two reasons: First, most device simulation software does not have the capability of considering photon recycling and therefore it is worth knowing under which circumstances this would lead to erroneous results. Second, the positive effect of photon recycling depends on the amount of parasitic absorption. If the solar cell is illuminating its own contact layers rather than its absorber layer, the result will be the creation of heat rather than the increase in the open-circuit voltage. This effect has been famously discussed in the context of thin-film GaAs solar cells.⁸⁰ Using thin layers of GaAs without a parasitically absorbing substrate and using high quality

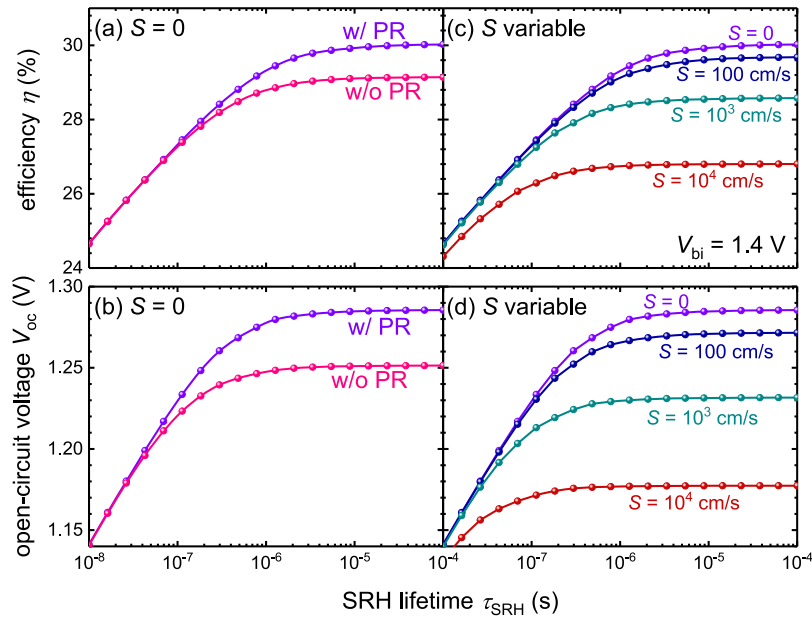


FIG. 6. (a) Efficiency and (b) open-circuit voltage as a function of SRH lifetime τ_{SRH} assuming perfectly passivated surfaces showing the effect of photon recycling using parameters presented in Table I. The curve labeled w/o PR excludes photon recycling and assumes that all bimolecular recombination is non-radiative, while the curve labeled w/ PR includes photon recycling and calculates the effect of reabsorption on the open-circuit voltage. Panels (c) and (d) show the same as panels (a) and (b) but now for different values of the surface recombination velocity S (always including photon recycling). Surface recombination velocities $S > 10$ cm/s will substantially affect V_{oc} in high quality lead-halide perovskite devices.

back reflectors increased the photovoltage of these devices relative to earlier implementations.⁸⁰ So far a clear relation between optical design and open-circuit voltage is still missing in perovskite solar cells, but the effects have been shown in films already.^{70,81} Figures 6(a) and 6(b) show the efficiency and open-circuit voltage as a function of SRH lifetime calculated using parameters listed in Table I. These results predict that the effect of photon recycling should matter for SRH lifetimes exceeding 300 ns which is a typical value for the transient photoluminescence lifetime of films on glass. However, in devices, surface recombination between the perovskite and the contact layers likely matters. Thus, Figs. 6(c) and 6(d) show the efficiency and open-circuit voltage as a function of SRH lifetime and using the surface recombination velocity as a parameter. We see that for surface recombination velocities $S \ll 100$ cm/s, the efficiency is close to the bulk limit, while any order of magnitude beyond $S = 100$ cm/s leads to a substantial decrease in efficiency and V_{oc} if high bulk lifetimes are reached. Clearly, the lower the bulk lifetime, the less important the surfaces become.

To clarify the significance of the different values of the surface recombination velocities used in the above calculations, a few words on experimental values of surface recombination velocities. While there is a large amount of data available on c-Si with values $S < 10$ cm/s being excellent,⁷⁵ so far relatively little quantitative data are available for lead-halide perovskites. Using transient reflectance spectroscopy, Yang *et al.*⁸² reported $S = 2800$ cm/s for single crystals and 450 cm/s for polycrystalline thin films that were both coated with polymethylmethacrylate (PMMA) for protection from the atmosphere. Using transient photoluminescence, Staub *et al.*⁴⁵ determined a surface recombination velocity $S < 10$ cm/s at the interface between MAPI and the glass substrate and at the bare MAPI surface (which is in essence an interface between MAPI and the N_2 in the cuvette used during the measurement), while Krogmeier *et al.*⁸³ determined $S \approx 200$ cm/s for a MAPI/PCBM interface. Brenes *et al.*⁸⁴ presented transient microwave photoconductivity measurements with low fluence lifetimes of ~ 30 μ s on 250 nm thick films treated by 30 min light soaking in humid air. These lifetimes correspond to surface recombination velocities not greater than $S = 0.4$ cm/s. Finally, Stolterfoht *et al.*⁷² determined surface recombination velocities of a mixed cation and mixed halide perovskite with poly(triaryl amine) and C_{60} to be about 26 cm/s each.

III. MICROSCOPIC UNDERSTANDING OF RECOMBINATION

In Sec. II, we have discussed how lifetimes, recombination coefficients, and surface recombination velocities affect the internal and external luminescence quantum efficiency, the open-circuit voltage, and finally the efficiency of a solar cell. We have also discussed typical values for lead-halide perovskites and compared them with those in Si. However, the discussion in Sec. II has been lacking so far a deeper understanding of what microscopic properties of a material in the bulk, at internal grain boundaries and interfaces with contact layers may affect these parameters.

Both the charge carrier lifetime in the bulk of a semiconductor and the surface recombination velocity S depend on the defect density N_T . In the case of the charge-carrier lifetime, the relationship is inverse and typically written as $\tau_{n/p} = (k_{n/p}N_T)^{-1}$. At surfaces, we may write $S_{n/p} = k_{s,n/p}N_S$ where N_S is the trap density per surface area and $k_{s,n/p}$ is the capture coefficient at the surface. Thus, in order to better understand lifetime and surface recombination velocity, we have to first discuss what we know about the defect density in the bulk or at interfaces and subsequently we have to discuss models for capture coefficients in semiconductors.

A. Defect densities

Defect densities in lead-halide perovskite films and crystals have been measured using a range of mostly electrical or optoelectronic techniques. Typical techniques to measure the energetic position and densities of defects are capacitance based techniques that rely on the storage of charge carriers on the defects.^{85,86} This storage of charge can be modulated by the applied DC voltage, the frequency, and the temperature. A frequently used method is, for instance, thermal admittance spectroscopy^{86,87} that is based on the variation of frequency and temperature. For any given temperature, there will be a characteristic frequency for a certain trap level. For lower frequencies f , the charge stored on the defect will contribute to the measured capacitance C , while for higher frequencies, the amount of charge stored on the defect cannot be modulated anymore with the AC voltage and the capacitance

will drop. Measuring these $C(f)$ steps at different temperatures then allows the translation of the frequency axis into an energy axis and the determination of the attempt-to-escape frequency which is directly related to the capture coefficient of electrons or holes. These capacitance steps were used, e.g., in Refs. 88 and 89 to measure defect densities and positions in lead-halide perovskites. Of course there are also other physical mechanisms such as buffer layers,⁹⁰ low mobilities,⁹¹ or ion-migration induced changes in electrostatics and therefore current flow that can induce frequency dependent steps in the capacitance and that may mistakenly be considered as defects. Thus, interpretation of thermal admittance spectroscopy data requires care and consideration of the signatures of different physical mechanisms.

A closely related technique is deep level transient spectroscopy (DLTS) developed by Lang⁹² in the 1970s that has been used for defect characterization in perovskites in Refs. 93 and 94 and that uses capacitance transients to extract densities, trap depths, and kinetic prefactors of defects. The thermally stimulated current (TSC) measurement^{95–98} is a third approach that is based on cooling a sample down, illuminating it to fill the defects with electrons, and then slowly warming the sample up while measuring the current. From the current as a function of time and therefore temperature, trap densities and depths may be obtained. Traps that are emptied and contribute to the current at lower temperatures must be shallow, while traps that require higher temperatures for trap release are deeper.

A completely different technique is a measurement of the current voltage curve of a unipolar device in a similar way as is performed in a space charge limited current measurement.⁹⁹ These measurements are often used in intrinsic low mobility materials to measure the mobility of electrons or holes.^{100,101} However, in the presence of defects, one may observe trap-limited currents that have a completely different voltage dependence than the space-charge-limited or the ohmic conduction that can be observed without traps.^{102,103} The voltage range, where trap-limited currents are observed, depends on the density of traps and can therefore be used as a measure of density but not of energetic position of traps.

Figure 7 summarizes the results reported in the literature on lead-halide perovskite films. There are essentially two types of presentations of the trap densities. Either the data are given as shown in Fig. 7(a) in total densities of defects per volume as a function of trap depth. Alternatively, the defect density is already integrated over energy or the method is only sensitive to the total density, as shown in Fig. 7(b).

Figure 7(a) shows data from Ref. 104 where passivation of the perovskite surface was performed with choline chloride and defect densities were reduced in the range accessible by thermal admittance spectroscopy. However, the data also show that midgap defects are in this case not accessible by the method. Studying deeper levels would require higher temperatures or lower frequencies either of

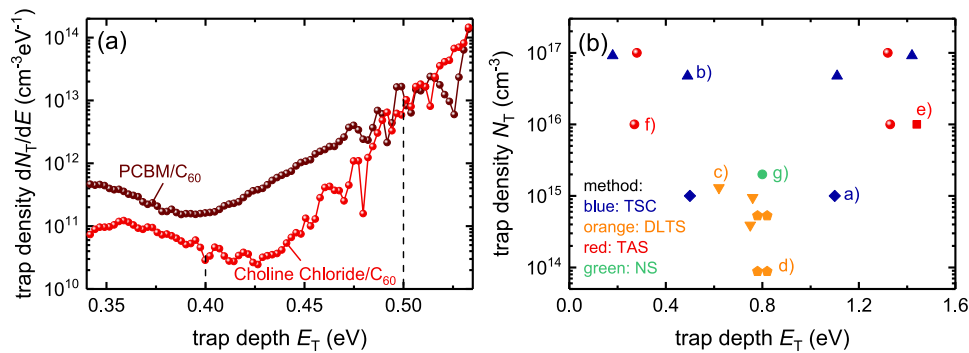


FIG. 7. (a) Trap density per energy interval as a function of trap depth E_T measured using thermal admittance spectroscopy on two different samples with and without choline chloride as a passivation layer. (b) Trap density as a function of trap depth for data reported in the literature and listed in Table II.^{88,89,93,94,98,154,155} Data in (b) are already integrated over energy, or the method is only sensitive to total trap density. In the cases where the trap depth can only be determined relative to the nearest band, we indicated the trap position twice (with respect to the conduction band at $E_T = 0$ and with respect to the valence band at $E_T = 1.6$ eV).

which cannot be changed infinitely. Higher temperatures will at some point destroy the perovskite layer, while lower frequencies might induce effects due to ion movement modulating recombination masking any effects due to detrapping of charge carriers.

Rather than giving an example, Fig. 7(b) is meant to give an overview over data presented in the literature. The data show that defect densities measured so far are primarily in the range of 10^{15} – 10^{16} cm $^{-3}$ with few exceptions of higher defect densities that are then, however, rather shallow. The x-axis in Fig. 7(b) has to be interpreted as showing the trap depth relative to the conduction band edge. If the references were able to identify whether the defect is closer to the conduction band than to the valence band, only one point is shown. If this is not known (as is usually the case), we added two data points that are symmetrically relative to midgap.

B. Chemical nature of defects

While defect densities and relative or absolute energetic depth with respect to bands as well as capture cross sections can be assessed experimentally (Fig. 7), it is often non-trivial to identify the chemical nature of the defect levels present in a device. The reason is that N_T is often so low that chemical imbalances are hard to detect by elemental specific methods. In addition, defects may not even be caused by any imbalance in chemical composition. For instance, an iodine interstitial is a defect that does not change the density of iodine atoms per cubic centimeter relative to a perfect crystal.

A common approach in semiconductor physics is to compare theoretically calculated energy levels and formation energies of defects that are likely to occur in the material.^{105,106} There are three different types of intrinsic defects, i.e., vacancies, interstitials, and antisites. Thus, in the case of MAPI, there are already twelve intrinsic defects possible, as shown in Fig. 8. These intrinsic defects are the three possible vacancies, the three interstitials, and six antisite defects. There have been several attempts to calculate the energetic position of defects using density functional theory^{107–113} that agree that a substantial number of the intrinsic defects are shallow but disagree in which ones are deep defects. Du¹⁰⁹ resolved this disagreement by comparing the energy levels of MAPI when calculated using different levels of theory in DFT. Particularly important for correct energy levels are the inclusion of spin-orbit coupling and the consideration of the self-interaction error that is high when using the generalized gradient approximation but partly removed when using hybrid density functional calculations.¹⁰⁹ This is illustrated in Fig. 8, where the frequently cited work of Yin *et al.*¹⁰⁷

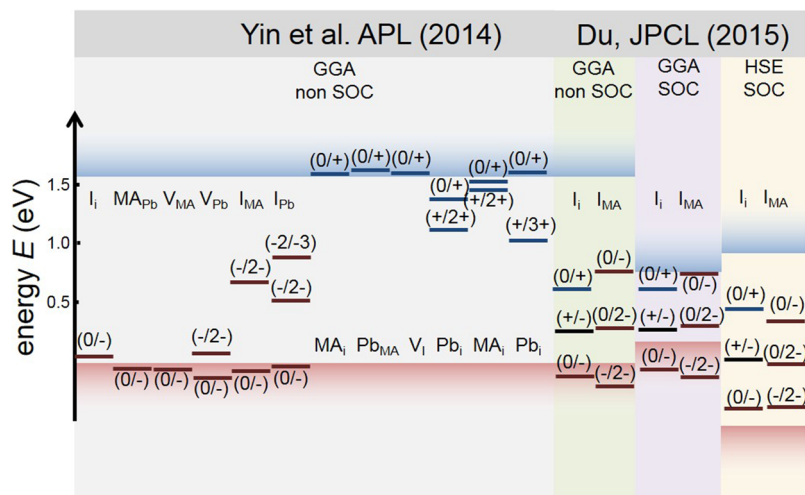


FIG. 8. Example for energy levels of intrinsic defects calculated for MAPI using density functional theory. The data on the left are taken from Ref. 107 and calculated with the generalized gradient approximation without spin-orbit coupling (GGA non-SOC). The data on the right are from Ref. 109 using (i) GGA non SOC, (ii) GGA with SOC (leading to substantially lower band gaps), and (iii) a hybrid functional with spin-orbit coupling (HSE SOC, HSE for Heyd-Scuseria-Ernzerhof¹⁵⁸) leading again to a realistic band gap. It is clear that the position of defect levels relative to the band edges depends considerably on the used functional and the inclusion or exclusion of spin-orbit coupling.

is shown on the left and the comparative calculations of Du¹⁰⁹ (for two representative defects) are shown on the right. The only remaining deep defects as shown in Fig. 8 (right) are then the iodine interstitial (I_i) and the related defect of iodine occupying a methylammonium position (I_{MA}).¹⁰⁹ This finding has triggered additional efforts to understand the behavior of iodine interstitials, their position as a function of their charge state,^{114,115} and the way their position is, for instance, affected by molecular oxygen¹¹⁶ or iodine.¹¹⁷

While the abovementioned papers all discuss bulk defects, surface defects might be of huge importance for the functionality of the perovskites in optoelectronic devices. Calculations of defects at surfaces have been performed by Uratani and Yamashita¹¹⁸ using the same functional as proposed by Du¹⁰⁹ and including spin-orbit coupling. They study the formation energy and position of defects at surfaces with different termination and under different growth conditions (I-rich, Pb-rich, or stoichiometric). Possible deep defects with low formation energies are iodine interstitials (same as bulk), Pb interstitials, and iodine vacancies. The authors also find that Pb-rich conditions are more favorable to suppress surface defects than I-rich conditions.

The low concentration of deep defects explains the frequently used term “defect tolerance”^{28,119} in the description of lead-halide perovskites. Defect tolerance is a term coined by the community working on computational and experimental material screening for potential novel solar cell absorber materials.¹²⁰ In the case of many typical semiconductors like Si, the valence band is formed of bonding orbitals, the conduction band is formed of antibonding orbitals, and any vacancy would lead to dangling bonds that have an energy in the band gap and therefore create deep defects. However, this is not always the case and in some semiconductors such as MAPbI₃, the valence band is formed from antibonding orbitals.^{28,105,121} The atomic orbitals, in this case I(5p), Pb(6s), and Pb(6p), are all outside the band gap or very close to the conduction band edge in the case of Pb(6p).²⁸ Upon formation of a lead vacancy, the surrounding iodide atoms form an acceptor level close to the valence band. For iodine vacancies, the remaining Pb atoms form a shallow donor defect level close to or in the conduction band.

Thus, while thin films of lead-halide perovskites are certainly not defect free, hardly any of the theoretically predicted intrinsic defects have an energetic position close to midgap allowing them to be highly recombination active. Shallow defects may, however, be abundant, in particular due to off-stoichiometric conditions during film formation¹²² or due to strain.¹²³ The shallow defects may trap electrons or holes but are not efficient at trapping both as we will discuss in Sec. III C. In addition, transient phenomena in experimental measurements such as the photoluminescence enhancement^{59,124} and hysteresis¹²⁵ indicate that charge-trapping ionic vacancies and interstitials may self-annihilate upon illumination and/or biasing. This complicates the experimental determination of defect energy levels, density, and chemical identity as defect distribution may change over time.

On top of this, these defects may dope the semiconductor *p*-type or *n*-type¹²² and defect diffusion through the film may thereby lead to changes in the electrical field distribution inside the absorber as a function of time after, e.g., voltage pulses^{126,127} or changes in light intensity.⁵⁹ What is also highly unclear is the role of (shallow) defects in the acceleration of degradation by either affecting the adsorption of water or oxygen molecules or enabling charge transfer.^{123,128}

C. Theory of non-radiative recombination

In Secs. III A and III B, we discussed the experimental evidence for defects and the theoretical expectations based on density functional theory. The defect density is an important factor in understanding and calculating charge-carrier lifetimes and surface recombination velocities. However, in addition to defect densities, also a kinetic prefactor is missing that is sometimes called a capture coefficient or which is alternatively given as the product of capture cross section and thermal velocity. This kinetic prefactor must depend on the ease with which thermal energy is dissipated in a certain crystal. Thus, we give a brief overview over the theoretical understanding of the kinetic terms involved in non-radiative recombination and apply this knowledge to the specific case of lead-halide perovskites.

Non-radiative transitions in semiconductors depend on the energetic separation between the initial and final state with larger separations $\Delta E \gg E_{\text{phon}}$ making transitions more unlikely as we will

learn below. Phonon energies E_{phon} are typically much smaller than the band gap, which makes direct transitions between the conduction and valence band unlikely. Thus, non-radiative recombination has to proceed via intermediate (defect) states that can capture both electrons from the conduction band and holes from the valence band efficiently. In order to fulfill the latter criterion, the defect states have to be close to the middle of the band gap, i.e., the defects have to be “deep” defects. Also half of the band gap is still much larger than the typical phonon energies, and therefore the conversion of electronic energy into nuclear vibrations requires the emission of multiple phonons. Thus, we want to briefly introduce the theory of multiphonon processes that has been developed since the 1950s by Huang and Rhys,¹²⁹ Gummel and Lax,¹³⁰ Kubo and Toyozawa,¹³¹ and others.^{132–135} More detailed discussions can be found in Refs. 136–138.

Let us assume we have a simple diatomic model of two atoms where the energy of the system is minimized for a given bond length. Any change in the bond length will lead to an increase in the total energy of the system that is in first order approximation described by a parabolic relation between energy and bond length. In a configuration coordinate diagram, we do not use the bond length but a more generic parameter—the configuration coordinate Q —as the x -axis but still work within a parabolic approximation. The shape of the parabola is defined by the phonon energy $E_{\text{phon}} = \hbar\omega$, and the energy of a given parabola centered at $Q = Q_i$ can be expressed as $E = E(Q_i) + \frac{1}{2} \omega^2 (Q - Q_i)^2$. Here \hbar is the reduced Planck’s constant, and ω is the angular frequency of the phonon.

If we now assume a band-like state (e.g., an electron in the conduction band) and a defect state, we will obtain two parabolas with the same shape that are shifted relative to each other both in energy and in Q , as shown in Fig. 9(a). The distance of the two minima of the parabolas in energy is the energy difference ΔE between (in this example) the bottom of the conduction band and the defect state. We can also express this energy difference in units of phonon energies. This number $p = \Delta E/\hbar\omega$ will become an important factor for the likelihood of recombination as we will see below. The amount of the shift

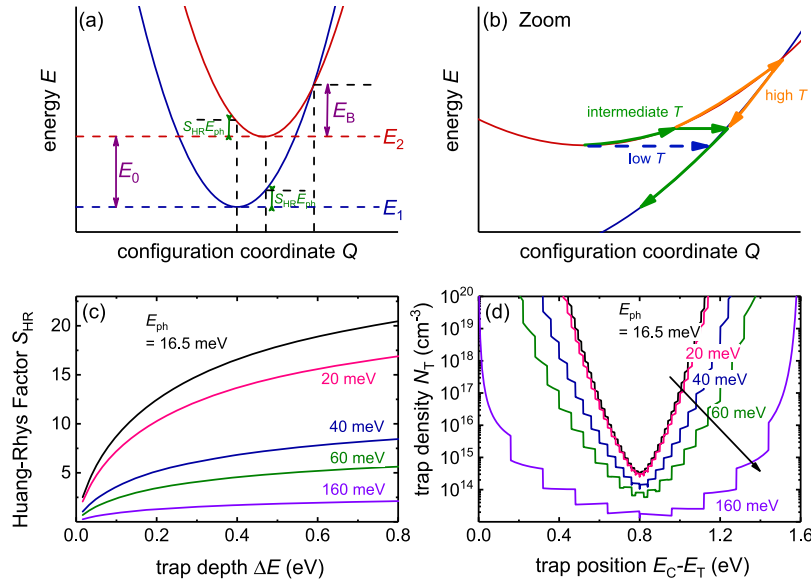


FIG. 9. (a) Configuration coordinate diagram illustrating the transition between two states. The upper parabola may represent the conduction band of semiconductor and the lower parabola a defect. Then for a non-radiative transition of an electron from the conduction band to the defect to happen, the electron needs to tunnel through the barrier amplified in (b) to a vibrationally excited state of the lower parabola. Depending on temperature, the transition between the two parabolas is due to a combination of thermal activation and tunneling. Note that only the high temperature limit of the transition is defined by the electron reaching the crossing point between the parabolas. (c) Huang-Rhys factors calculated for polar coupling according to Eq. (15) for different values of the phonon energy keeping the frequency dependent permittivity and the lattice constant the same (using the values of MAPI in Table III). (d) Using the theory of tunneling through the barrier in (b) formed by two parabolas, we obtain capture coefficients that dictate the relation between SRH lifetime and trap density. Panel (d) then shows the trap density necessary to reach a SRH lifetime of 1 μs . Panels (c) and (d) are reproduced with permission from Kirchartz *et al.*, J. Phys. Chem. Lett. 9, 939 (2018). Copyright 2018 The American Chemical Society.

in Q depends on the so-called Huang-Rhys factor S_{HR} that describes the strength of electron-phonon coupling with higher values of S_{HR} implying stronger electron-phonon coupling. Any non-radiative transition between the two parabolas has to occur by tunneling and/or thermal excitation from the upper parabola to a vibrationally excited state of the lower parabola. Figure 9(b) shows a zoomed-in version of Fig. 9(a) illustrating how temperature affects the transition. At high temperatures, the electron may reach the crossing point leading to the classical high temperature limit of non-radiative transitions that is thermally activated with the energy barrier $E_B = (\Delta E - S_{\text{HR}}\hbar\omega)^2 / (4S_{\text{HR}}\hbar\omega)$ at the crossing point being the activation energy. At lower temperatures, the transition will have to involve tunneling between the parabolas. If one calculates the tunneling rate through a barrier formed by two parabolas, as shown in Fig. 9(b), the multiphonon transition rate can be calculated over the whole range of temperatures. References 134, 136, and 139 describe the capture coefficient $k_{\text{n/p}}$ (in units cm^3/s) as

$$k_{\text{n/p}} = \frac{V_T p^2 \omega \sqrt{2\pi}}{\sqrt{p\sqrt{1+x^2}}} \exp \left[p \left(\frac{\hbar\omega}{2kT} + \sqrt{1+x^2} - x \cosh \left(\frac{\hbar\omega}{2kT} \right) - \ln \left(\frac{1 + \sqrt{1+x^2}}{x} \right) \right) \right], \quad (13)$$

using¹⁴⁰

$$x = \begin{cases} \frac{S_{\text{HR}}}{p \sinh(\hbar\omega/2kT)} & \text{for } S_{\text{HR}} < p \\ \frac{p}{S_{\text{HR}} \sinh(\hbar\omega/2kT)} & \text{for } S_{\text{HR}} > p \end{cases}. \quad (14)$$

Here, V_T is the volume of the defect which is assumed to be a sphere with the radius $a^*v/2$, where a^* is the effective Bohr radius and $v = q(8\pi\epsilon a^* \Delta E)^{-1/2}$. This assumption for the radius of the defect wavefunction is based on the quantum defect model and guarantees that deep defects will have a smaller wavefunction radius than shallower defects. Of course, the model is a generic model that does not take into account the specific properties of a particular defect. Please note that Eq. (13) is based on the tunneling probability through the barrier shown in Fig. 9(b) and it is strongly dependent on the value of p . Higher values of p strongly reduce the tunneling probability and therefore the capture coefficient k .

In order to estimate a value of the transition rate for lead-halide perovskites, we need a way of estimating how the parabolas are shifted relative to each other, i.e., we need to know the Huang-Rhys factor. The Huang-Rhys factor has been determined experimentally for defects in GaAs and GaP by Henry and Lang,¹³⁵ but there are no experimental data available for defects in lead-halide perovskites. The Huang-Rhys factor will also depend on the specific properties of the trap and will be different for shallow and deep traps. From a theoretical point of view, the Huang-Rhys factor depends on the different types of electron phonon coupling in a crystal, namely, deformation coupling and polar coupling,¹⁴¹ both of which depend on the frequency dependent permittivity of the material. Ridley provides equations that allow a theoretical estimate of the Huang-Rhys factor for both mechanisms. However, for deformation coupling, the equation requires the knowledge of the deformation coupling constant which expresses the change in the energy levels as a function of displacement of atoms relative to their equilibrium position (in $\text{eV}/\text{\AA}$). This optical deformation potential constant is rather difficult to determine experimentally and theoretically.¹⁴² For lead-halide perovskites, no information on this constant is available and thus, the Huang-Rhys factor for optical deformation coupling cannot currently be estimated. However, given that lead-halide perovskites are polar semiconductors, it is fair to assume that polar coupling is dominant. Here all necessary information is available, and therefore, the Huang-Rhys factor for polar coupling can be estimated using the equations provided by Ridley,^{132,141}

$$S_{\text{HR}} = \frac{3}{2(\hbar\omega)^2} \left\{ \frac{q^2 a_0^{-3} \hbar\omega^2}{\omega q_D^2} \left(\frac{1}{\epsilon_\infty} - \frac{1}{\epsilon} \right) \right\} I(-2, 2\mu, q_D a^* v/2). \quad (15)$$

Here, $q_D = (6\pi^2)^{1/3}/a_0$, a_0 is the lattice constant, ϵ_∞ and ϵ are the high- and low-frequency limit of the permittivity, μ and ν are defined in Table II, and I is defined via

TABLE II. Trap density as a function of trap depth for data reported in the literature and presented in Fig. 7(b). If two values of the trap depth are given in the same row, then only the depth relative to the closest band is known but not whether the band is the conduction band or the valence band. The values are generally given relative to the conduction band ($E_T = 0$). The valence band is assumed to be at $E_T = 1.6$ eV.

Method		Reference	Trap depth E_T (eV)	Trap density (cm^{-3})
Thermally stimulated current (TSC)	(a)	Baumann <i>et al.</i> ¹⁵⁴	0.5/1.1	$>10^{15}$
	(b)	Gordillo <i>et al.</i> ⁹⁸	0.18/1.42	9.14×10^{16}
			0.49/1.11	4.75×10^{16}
Deep level transient spectroscopy (DLTS)	(c)	Heo <i>et al.</i> ⁹³	0.62	1.3×10^{15}
			0.75	3.9×10^{14}
			0.76	9.5×10^{14}
	(d)	Yang <i>et al.</i> ⁹⁴	0.78/0.82	8.81×10^{13}
			0.78/0.82	5.28×10^{14}
Thermal admittance spectroscopy (TAS)	(e)	Duan <i>et al.</i> ⁸⁸	1.44	$\sim 10^{16}$
	(f)	Heo <i>et al.</i> ⁸⁹	0.27/1.33	10^{16}
			0.28/1.32	10^{17}
Noise spectroscopy (NS)	(g)	Landi <i>et al.</i> ¹⁵⁵	0.8	2×10^{15}

$$I(a, b, c) = \frac{1}{(bc)^2} \int_0^1 \frac{x^a \sin^2(b \tan^{-1}(cx))}{[1 + (cx)^2]^b} dx. \quad (16)$$

Figure 9(c) shows the Huang-Rhys factor resulting from Eqs. (15) and (16) in conjunction with the parameters given in Table III for MAPI. The LO phonon energy of MAPI is 16.5 meV¹⁴³ leading to the highest values of S_{HR} . For deeper traps, the wavefunction becomes more localized and therefore S_{HR} increases. If we increase the phonon energy in a gedanken experiment without changing any other parameter, the Huang-Rhys factor drops as predicted by Eq. (15). Figure 9(d) shows now the necessary trap density to achieve a SRH lifetime of 1 μs if we insert the values for $k_{\text{n/p}}$ given in Eq. (13) into the SRH recombination rate and if we use the Huang-Rhys factors given in panel (c). Midgap traps require lower defect densities because they minimize the largest single transition that has to be made. If the defect is below or above midgap, one of the transitions requires

TABLE III. Parameter and abbreviations used in the calculations shown in Figs. 9(c) and 9(d). The simulations were performed assuming a temperature $T = 300$ K. Reproduced and modified with permission from Kirchartz *et al.*, J. Phys. Chem. Lett. 9, 939 (2018). Copyright 2018 The American Chemical Society.

Parameter	Symbol or equation	Value
Phonon energy	$E_{\text{ph}} = \hbar\omega$	16.5 meV (LO phonon) ¹⁴³
Reduced mass	$M_r = M_{\text{Pb}}M_{\text{I}}/(M_{\text{Pb}} + M_{\text{I}})$	78.7 Da
Permittivity(frequency)	$\epsilon(f)$	$\epsilon(0) = 33.5\epsilon_0$ $\epsilon(\infty) = 5.0\epsilon_0$ ¹⁴³
Lattice constant	a_0	6.3 Å ¹⁵⁶
Radius of sphere with Brillouin zone volume	$q_D = (6\pi^2)^{1/3}/a_0$	6.2 nm ⁻¹
Effective mass	m_{eff}	0.2 (assumed equal for electrons and holes)
Bohr radius	$a_H = 4\pi\epsilon_0\hbar^2/mq^2$	5.292×10^{-2} nm
Effective Bohr radius	$a^* = a_H \epsilon_r(0)/m_{\text{eff}}$	8.9 nm
Rydberg energy	$R_H = q^2/(8\pi\epsilon_0 a_H)$	13.605 eV
Effective Rydberg energy	$R^* = q^2/(8\pi\epsilon(0)a^*)$	2.4 meV
	$\nu = q(8\pi\epsilon(0)a^*\Delta E)^{-1/2}$	Variable
	$\mu = \begin{cases} \nu & \text{for positively charged defects} \\ 0 & \text{for neutral defects} \\ -\nu & \text{for negatively charged defects} \end{cases}$	
Sommerfeld factor ¹⁵⁷	$s_a = 4(\pi R^*/kT)^{1/2}$	2.2
Temperature	$T = 300$ K	

a higher and one a lower number of phonons. Because the transition rate decreases strongly with increasing numbers of phonons, the transition with the higher number of phonons is less likely, and because recombination is a series connection of two capture processes, the slower of the two will limit the rate. Thus, deep defects are more detrimental. However, the sensitivity of the recombination rate to a change in defect position is much higher if the phonon energy is lower. Thus, for polar materials with heavier elements (like MAPI) and lower phonon energies, the sensitivity of the recombination rate to the position of the defect is higher and the tolerance toward defects that are not midgap is substantially higher than for classical semiconductors with slightly higher phonon energies.¹³⁹

IV. OPEN QUESTIONS

There are a range of open questions associated with recombination and open-circuit voltage in lead-halide perovskites that deserve the attention of the research community. In this review, we have discussed possible reasons why non-radiative bulk recombination is slow in lead-halide perovskites. This slow bulk recombination, however, just moves the problem to the surfaces and interfaces that have to exist in any solar cell. While we discussed the impact of increasing the surface recombination velocity S in the context of Figs. 4 and 5, however, microscopic understanding of surface recombination is still missing. Many contact materials were successfully used with lead-halide perovskites to achieve at least decent photovoltaic efficiencies and V_{oc} s. This suggests that making high electronic quality interfaces might be less of a problem than, for instance, in Si or GaAs. However, for future high efficiency large area devices made from lead-halide perovskites, we need to identify the electron and hole contact layers with the highest possible efficiency potential and even low levels of recombination may be limiting further efficiency improvements. Thus, it is worth asking fundamental questions that will help us to better understand interfacial recombination. An obvious question is how to treat recombination of, e.g., an electron in an electron transport material like PCBM with a hole in the perovskite.⁸³ This is interesting, in particular, due to the fact that many electron and hole transport layers used are organic semiconductors which feature much higher vibrational energies⁶⁸ than the halide perovskites which are being built up by much heavier elements (leading to lower phonon energies). Thus, it is unclear (at least to the authors) how energy dissipation at such an organic-inorganic interface would work and how much of a possibly detrimental influence the higher energy vibrational modes in the organic layers have. Currently, the high open-circuit voltages achieved with organic electron and hole transport layers^{104,144} suggest that there are situations possible with very little detrimental influence.

Many recent publications on improving photovoltaic power conversion efficiency or luminescence yield in lead-halide perovskites studied the effect of altering the properties of the film surfaces/interfaces rather than the bulk.^{70,104,145–149} In these papers, it is often implied that the technological change leading to higher performance was due to “surface passivation” or a reduction in the interfacial defect density. An obvious question is whether it actually always is the reduction in the defect density in a similar way as performed in the case of interfaces of a Si crystal and a passivation layer or whether contact layers may actually keep the defect density the same and still slow down recombination. There are various alternative ways such as changing the capture coefficients via changing the electron-phonon coupling or the energy of the phonons available for recombination. The reduction in surface recombination can also be achieved by slowing down majority and minority carrier extraction at an interface via, e.g., point contacts or tunneling contacts. This is a standard way of reducing losses at interfaces in Si solar cells, where the selectivity of the interface layer remains the same. However, situations may exist where increasing the series resistance at an interface does not affect efficiency (e.g., because the series resistance is limited by another process), while reducing surface recombination would increase the efficiency (e.g., because it does limit V_{oc}).¹⁵⁰

Another open question related to the theory of recombination is the limit of the harmonic approximation. There are a range of publications^{151–153} that discuss evidence for the harmonic approximation to be insufficient to explain experimental data, in particular for mobility measurements. Yaffe *et al.*¹⁵³ noted that the presence of a central peak toward low energies (or wavenumbers) in Raman spectra is clear evidence of anharmonicity. One of the main open questions is how this anharmonicity would

affect the theory of multiphonon recombination described above. This problem cannot be tackled anymore in a generic way as performed above but requires the calculation of wavefunctions for actual defects.

V. SUMMARY

Understanding the open-circuit voltage of a solar cell is a challenge that requires a deep understanding of the different recombination mechanisms that occur in the bulk and at surfaces of the absorber material. In the case of lead-halide perovskites, the non-radiative recombination is relatively slow compared to the (fairly fast) radiative recombination. This is a desirable condition for a solar cell because it allows low thicknesses for full absorption due to the fast radiative recombination (implying a high absorption coefficient), while non-radiative decay does not add huge additional losses in the voltage at open circuit or the maximum power point. This condition has several implications: (i) mobilities should not matter very much. Even the fairly low mobilities of lead-halide perovskites (if compared to Si or GaAs) are high enough. (ii) If the bulk features slow non-radiative recombination, the surfaces should matter and it is therefore not surprising how many recent publications are dedicated to reducing recombination at surfaces and interfaces. (iii) If the bulk of the material is close to the radiative limit (i.e., the non-radiative losses are small), optical effects like photon recycling will become increasingly important and in consequence also the optical design of the layer stack.

In addition to these implications of slow non-radiative recombination in lead-halide perovskites, this fact also raises a couple of questions, in particular how to explain this slow recombination. The explanation we provide here is based on the theory of multiphonon recombination which states that the combination of polar materials, high masses, and therefore low phonon energies and fairly decent densities of deep defects is a desirable condition for slow non-radiative recombination. In such a semiconductor, fairly large defect densities that are not midgap should be tolerable as long as there are no trap to trap transitions possible. How this theory can be extended to surfaces and interfaces and how far the effects of anharmonicity will affect non-radiative recombination are the main open questions that require further attention from a theoretical perspective.

ACKNOWLEDGMENTS

The authors acknowledge support from the Impuls- und Vernetzungsfonds der Helmholtz Gemeinschaft via the project PEROSEED. T.K. and L.K. thank the Bavarian Ministry of Economic Affairs and Media, Energy and Technology for the joint projects in the framework of the Helmholtz Institute Erlangen-Nürnberg. E.L.U. acknowledges funding from the Swedish Research Council (Project No. 2015-00163) and Marie Skłodowska Curie Actions, Cofund, Project No. INCA 600398, and the German Ministry of Education and Research (BMBF) for the Young Investigator Group Hybrid Materials Formation and Scaling (HyPerFORME) within the program “NanoMatFutur” (Grant No. 03XP0091).

- ¹ G. E. Eperon, M. T. Hörantner, and H. J. Snaith, *Nat. Rev. Chem.* **1**, 0095 (2017).
- ² W. Zhang, G. E. Eperon, and H. J. Snaith, *Nat. Energy* **1**, 16048 (2016).
- ³ S. D. Stranks and H. J. Snaith, *Nat. Nanotechnol.* **10**, 391 (2015).
- ⁴ M. A. Green, A. Ho-Baillie, and H. J. Snaith, *Nat. Photonics* **8**, 506 (2014).
- ⁵ J. P. Correa-Baena, M. Saliba, T. Buonassisi, M. Grätzel, A. Abate, W. Tress, and A. Hagfeldt, *Science* **358**, 739 (2017).
- ⁶ B. R. Sutherland and E. H. Sargent, *Nat. Photonics* **10**, 295 (2016).
- ⁷ C. Zuo, H. J. Bolink, H. Han, J. Huang, D. Cahen, and L. Ding, *Adv. Sci.* **3**, 1500324 (2016).
- ⁸ Q. A. Akkerman, G. Raino, M. V. Kovalenko, and L. Manna, *Nat. Mater.* **17**, 394 (2018).
- ⁹ M. A. Becker, R. Vaxenburg, G. Nedelcu, P. C. Sercel, A. Shabaev, M. J. Mehl, J. G. Michopoulos, S. G. Lambrakos, N. Bernstein, J. L. Lyons *et al.*, *Nature* **553**, 189 (2018).
- ¹⁰ M. V. Kovalenko, L. Protesescu, and M. I. Bodnarchuk, *Science* **358**, 745 (2017).
- ¹¹ H. Wei, D. DeSantis, W. Wei, Y. Deng, D. Guo, T. J. Savenije, L. Cao, and J. Huang, *Nat. Mater.* **16**, 826 (2017).
- ¹² J. Huang, Y. Yuan, Y. Shao, and Y. Yan, *Nat. Rev. Mater.* **2**, 17042 (2017).
- ¹³ W. Wei, Y. Zhang, Q. Xu, H. Wei, Y. Fang, Q. Wang, Y. Deng, T. Li, A. Gruverman, L. Cao *et al.*, *Nat. Photonics* **11**, 315 (2017).
- ¹⁴ H. H. Fang, S. Adjokatse, H. Wei, J. Yang, G. R. Blake, J. Huang, J. Even, and M. A. Loi, *Sci. Adv.* **2**, e1600534 (2016).
- ¹⁵ Z. Xiao and J. Huang, *Adv. Electron. Mater.* **2**, 1600100 (2016).

- ¹⁶ M. A. Green, Y. Hishikawa, E. D. Dunlop, D. H. Levi, J. Hohl-Ebinger, and A. W. Y. Ho-Baillie, *Prog. Photovoltaics: Res. Appl.* **26**, 3 (2018).
- ¹⁷ K. Yoshikawa, H. Kawasaki, W. Yoshida, T. Irie, K. Konishi, K. Nakano, T. Uto, D. Adachi, M. Kanematsu, H. Uzu *et al.*, *Nat. Energy* **2**, 17032 (2017).
- ¹⁸ A. V. Shah, H. Schade, M. Vaneccek, J. Meier, E. Vallat-Sauvain, N. Wyrsch, U. Kroll, C. Droz, and J. Bailat, *Prog. Photovoltaics: Res. Appl.* **12**, 113 (2004).
- ¹⁹ H. Li, Z. Xiao, L. Ding, and J. Wang, *Sci. Bull.* **63**, 340 (2018).
- ²⁰ X. Che, Y. Li, Y. Qu, and S. R. Forrest, *Nat. Energy* **3**, 422 (2018).
- ²¹ P. Jackson, R. Wuerz, D. Hariskos, E. Lotter, W. Witte, and M. Powalla, *Phys. Status Solidi RRL* **10**, 583 (2016).
- ²² P. Jackson, D. Hariskos, R. Wuerz, O. Kiowski, A. Bauer, T. M. Friedlmeier, and M. Powalla, *Phys. Status Solidi RRL* **9**, 28 (2015).
- ²³ F. Pianezzi, P. Reinhard, A. Chirila, B. Bissig, S. Nishiwaki, S. Buecheler, and A. N. Tiwari, *Phys. Chem. Chem. Phys.* **16**, 8843 (2014).
- ²⁴ S. Siebentritt, *Curr. Opin. Green Sustainable Chem.* **4**, 1 (2017).
- ²⁵ M. Saliba, T. Matsui, K. Domanski, J. Y. Seo, A. Ummadisingu, S. M. Zakeeruddin, J. P. Correa-Baena, W. R. Tress, A. Abate, A. Hagfeldt *et al.*, *Science* **354**, 206 (2016).
- ²⁶ W. Tress, *Adv. Energy Mater.* **7**, 1602358 (2017).
- ²⁷ D. A. Egger, A. Bera, D. Cahen, G. Hodes, T. Kirchartz, L. Kronik, R. Lovrincic, A. M. Rappe, D. R. Reichman, and O. Yaffe, *Adv. Mater.* **30**, 1800691 (2018).
- ²⁸ R. E. Brandt, V. Stevanović, D. S. Ginley, and T. Buonassisi, *MRS Commun.* **5**, 265 (2015).
- ²⁹ B. Blank, T. Kirchartz, S. Lany, and U. Rau, *Phys. Rev. Appl.* **8**, 024032 (2017).
- ³⁰ T. Kirchartz and U. Rau, *Adv. Energy Mater.* **8**, 1703385 (2018).
- ³¹ U. Rau, *Phys. Rev. B* **76**, 085303 (2007).
- ³² M. A. Green, J. H. Zhao, A. H. Wang, P. J. Reece, and M. Gal, *Nature* **412**, 805 (2001).
- ³³ R. T. Ross, *J. Chem. Phys.* **46**, 4590 (1967).
- ³⁴ G. Smestad and H. Ries, *Sol. Energy Mater. Sol. Cells* **25**, 51 (1992).
- ³⁵ U. Rau, B. Blank, T. C. M. Müller, and T. Kirchartz, *Phys. Rev. Appl.* **7**, 044016 (2017).
- ³⁶ W. Shockley and H. J. Queisser, *J. Appl. Phys.* **32**, 510 (1961).
- ³⁷ J. Z. Yao, T. Kirchartz, M. S. Vezie, M. A. Faist, W. Gong, Z. C. He, H. B. Wu, J. Troughton, T. Watson, D. Bryant *et al.*, *Phys. Rev. Appl.* **4**, 014020 (2015).
- ³⁸ T. C. M. Müller, B. E. Pieters, T. Kirchartz, R. Carius, and U. Rau, *Sol. Energy Mater. Sol. Cells* **129**, 95 (2014).
- ³⁹ R. A. Street, D. K. Biegelsen, and R. L. Weisfield, *Phys. Rev. B* **30**, 5861 (1984).
- ⁴⁰ R. A. Street, *Adv. Phys.* **30**, 593 (1981).
- ⁴¹ W. Shockley and W. T. Read, *Phys. Rev.* **87**, 835 (1952).
- ⁴² R. N. Hall, *Phys. Rev.* **87**, 387 (1952).
- ⁴³ U. Rau, U. W. Paetzold, and T. Kirchartz, *Phys. Rev. B* **90**, 035211 (2014).
- ⁴⁴ American Society for Testing and Materials, NREL, Golden, Colorado, 2017.
- ⁴⁵ F. Staub, H. Hempel, J. C. Hebig, J. Mock, U. W. Paetzold, U. Rau, T. Unold, and T. Kirchartz, *Phys. Rev. Appl.* **6**, 044017 (2016).
- ⁴⁶ R. Brendel and H. J. Queisser, *Sol. Energy Mater. Sol. Cells* **29**, 397 (1993).
- ⁴⁷ T. Kirchartz, F. Staub, and U. Rau, *ACS Energy Lett.* **1**, 731 (2016).
- ⁴⁸ I. Zonno, B. Krogmeier, V. Katte, D. Lübke, A. Martinez-Otero, and T. Kirchartz, *Appl. Phys. Lett.* **109**, 183301 (2016).
- ⁴⁹ T. Kirchartz and U. Rau, *Sustainable Energy Fuels* **2**, 1550 (2018).
- ⁵⁰ M. A. Green, *Prog. Photovoltaics: Res. Appl.* **10**, 235 (2002).
- ⁵¹ J. Mattheis, J. H. Werner, and U. Rau, *Phys. Rev. B* **77**, 085203 (2008).
- ⁵² T. Kirchartz and U. Rau, *J. Phys. Chem. Lett.* **8**, 1265 (2017).
- ⁵³ T. Kirchartz, J. Bisquert, I. Mora-Sero, and G. Garcia-Belmonte, *Phys. Chem. Chem. Phys.* **17**, 4007 (2015).
- ⁵⁴ S. D. Stranks, V. M. Burlakov, T. Leijtens, J. M. Ball, A. Goriely, and H. J. Snaith, *Phys. Rev. Appl.* **2**, 034007 (2014).
- ⁵⁵ S. D. Stranks, G. E. Eperon, G. Grancini, C. Menelaou, M. J. P. Alcocer, T. Leijtens, L. M. Herz, A. Petrozza, and H. J. Snaith, *Science* **342**, 341 (2013).
- ⁵⁶ D. Bi, W. Tress, M. I. Dar, P. Gao, J. Luo, C. Renevier, K. Schenk, A. Abate, F. Giordano, J. P. Correa Baena *et al.*, *Sci. Adv.* **2**, e1501170 (2016).
- ⁵⁷ D. W. deQuilettes, S. M. Vorpahl, S. D. Stranks, H. Nagaoka, G. E. Eperon, M. E. Ziffer, H. J. Snaith, and D. S. Ginger, *Science* **348**, 683 (2015).
- ⁵⁸ M. Abdi-Jalebi, Z. Andaji-Garmaroudi, S. Cacovich, C. Stavrakas, B. Philippe, J. M. Richter, M. Alsari, E. P. Booker, E. M. Hutter, A. J. Pearson *et al.*, *Nature* **555**, 497 (2018).
- ⁵⁹ D. W. deQuilettes, W. Zhang, V. M. Burlakov, D. J. Graham, T. Leijtens, A. Osherov, V. Bulovic, H. J. Snaith, D. S. Ginger, and S. D. Stranks, *Nat. Commun.* **7**, 11683 (2016).
- ⁶⁰ D. W. deQuilettes, S. Koch, S. Burke, R. K. Paranjhi, A. J. Shropshire, M. E. Ziffer, and D. S. Ginger, *ACS Energy Lett.* **1**, 438 (2016).
- ⁶¹ L. M. Herz, *ACS Energy Lett.* **2**, 1539 (2017).
- ⁶² T. M. Brenner, D. A. Egger, A. M. Rappe, L. Kronik, G. Hodes, and D. Cahen, *J. Phys. Chem. Lett.* **6**, 4754 (2015).
- ⁶³ S. D. Stranks, *ACS Energy Lett.* **2**, 1515 (2017).
- ⁶⁴ F. Ambrosio, J. Wiktor, F. De Angelis, and A. Pasquarello, *Energy Environ. Sci.* **11**, 101 (2018).
- ⁶⁵ P. W. Bridgman, *Phys. Rev.* **31**, 101 (1928).
- ⁶⁶ W. van Roosbroeck and W. Shockley, *Phys. Rev.* **94**, 1558 (1954).
- ⁶⁷ K. Vandewal, K. Tvingstedt, A. Gadisa, O. Inganäs, and J. V. Manca, *Nat. Mater.* **8**, 904 (2009).

- ⁶⁸ J. Benduhn, K. Tvingstedt, F. Piersimoni, S. Ullbrich, Y. Fan, M. Tropiano, K. A. McGarry, O. Zeika, M. K. Riede, C. J. Douglas *et al.*, *Nat. Energy* **2**, 17053 (2017).
- ⁶⁹ T. Kirchartz, P. Kaienburg, and D. Baran, *J. Phys. Chem. C* **122**, 5829 (2018).
- ⁷⁰ I. L. Braly, D. W. deQuilettes, L. M. Pazos-Outon, S. Burke, M. E. Ziffer, D. S. Ginger, and H. W. Hillhouse, *Nat. Photonics* **12**, 355 (2018).
- ⁷¹ F. Staub, U. Rau, and T. Kirchartz, *ACS Omega* **3**, 8009 (2018).
- ⁷² M. Stolterfoht, C. M. Wolff, J. A. Marquez, S. Zhang, C. J. Hages, D. Rothhardt, S. Albrecht, P. L. Burn, P. Meredith, T. Unold *et al.*, *Nat. Energy* **3**, 847–854 (2018).
- ⁷³ P. P. Altermatt, *J. Comput. Electron.* **10**, 314 (2011).
- ⁷⁴ A. Richter, M. Hermle, and S. W. Glunz, *IEEE J. Photovoltaics* **3**, 1184 (2013).
- ⁷⁵ A. Richter, S. W. Glunz, F. Werner, J. Schmidt, and A. Cuevas, *Phys. Rev. B* **86**, 165202 (2012).
- ⁷⁶ T. Tiedje, E. Yablonovitch, G. D. Cody, and B. G. Brooks, *IEEE Trans. Electron Devices* **31**, 711 (1984).
- ⁷⁷ M. A. Green, *IEEE Trans. Electron Devices* **31**, 671 (1984).
- ⁷⁸ L. M. Pazos-Outon, T. P. Xiao, and E. Yablonovitch, *J. Phys. Chem. Lett.* **9**, 1703 (2018).
- ⁷⁹ J. Mattheis, *Mobility and Homogeneity Effects on the Power Conversion Efficiency of Solar Cells* (Universität Stuttgart, 2008), p. 140.
- ⁸⁰ O. D. Miller, E. Yablonovitch, and S. R. Kurtz, *IEEE J. Photovoltaics* **2**, 303 (2012).
- ⁸¹ F. Staub, T. Kirchartz, K. Bittkau, and U. Rau, *J. Phys. Chem. Lett.* **8**, 5084 (2017).
- ⁸² Y. Yang, M. Yang, D. Moore, Y. Yan, E. Miller, K. Zhu, and M. Beard, *Nat. Energy* **2**, 16207 (2017).
- ⁸³ B. Krogmeier, F. Staub, D. Grabowski, U. Rau, and T. Kirchartz, *Sustainable Energy Fuels* **2**, 1027 (2018).
- ⁸⁴ R. Brenes, D. Guo, A. Osherov, N. K. Noel, C. Eames, E. M. Hutter, S. K. Pathak, F. Niroui, R. H. Friend, M. S. Islam *et al.*, *Joule* **1**, 155 (2017).
- ⁸⁵ A. R. Peaker, V. P. Markevich, and J. Coutinho, *J. Appl. Phys.* **123**, 161559 (2018).
- ⁸⁶ J. Heath and P. Zabierowski, in *Advanced Characterization Techniques for Thin Film Solar Cells*, edited by D. Abou-Ras, T. Kirchartz, and U. Rau (Wiley-Vch, Weinheim, 2011), p. 81.
- ⁸⁷ T. Walter, R. Herberholz, C. Müller, and H. W. Schock, *J. Appl. Phys.* **80**, 4411 (1996).
- ⁸⁸ H. S. Duan, H. Zhou, Q. Chen, P. Sun, S. Luo, T. B. Song, B. Bob, and Y. Yang, *Phys. Chem. Chem. Phys.* **17**, 112 (2015).
- ⁸⁹ J. H. Heo, D. H. Song, H. J. Han, S. Y. Kim, J. H. Kim, D. Kim, H. W. Shin, T. K. Ahn, C. Wolf, T.-W. Lee *et al.*, *Adv. Mater.* **27**, 3424 (2015).
- ⁹⁰ F. Werner and S. Siebentritt, *Phys. Rev. Appl.* **9**, 054047 (2018).
- ⁹¹ S. Wang, P. Kaienburg, B. Klingebiel, D. Schillings, and T. Kirchartz, *J. Phys. Chem. C* **122**, 9795 (2018).
- ⁹² D. V. Lang, *J. Appl. Phys.* **45**, 3023 (1974).
- ⁹³ S. Heo, G. Seo, Y. Lee, D. Lee, M. Seol, J. Lee, J. B. Park, K. Kim, D. J. Yun, Y. S. Kim *et al.*, *Energy Environ. Sci.* **10**, 1128 (2017).
- ⁹⁴ W. S. Yang, B. W. Park, E. H. Jung, N. J. Jeon, Y. C. Kim, D. U. Lee, S. S. Shin, J. Seo, E. K. Kim, J. H. Noh *et al.*, *Science* **356**, 1376 (2017).
- ⁹⁵ R. Schmechel and H. von Seggern, *Phys. Status Solidi A* **201**, 1215 (2004).
- ⁹⁶ J. Schafferhans, A. Baumann, C. Deibel, and V. Dyakonov, *Appl. Phys. Lett.* **93**, 093303 (2008).
- ⁹⁷ J. Schafferhans, C. Deibel, and V. Dyakonov, *Adv. Energy Mater.* **1**, 655 (2011).
- ⁹⁸ G. Gordillo, C. A. Otalora, and M. A. Reinoso, *J. Appl. Phys.* **122**, 075304 (2017).
- ⁹⁹ A. Rose, *Phys. Rev.* **97**, 1538 (1955).
- ¹⁰⁰ Z. M. Bailey, E. T. Hoke, R. Noriega, J. Dacuna, G. F. Burkhard, J. A. Bartelt, A. Salleo, M. F. Toney, and M. D. McGehee, *Adv. Energy Mater.* **1**, 954 (2011).
- ¹⁰¹ J. A. Röhr, X. Shi, S. A. Haque, T. Kirchartz, and J. Nelson, *Phys. Rev. Appl.* **9**, 044017 (2018).
- ¹⁰² M. A. Lampert, *Phys. Rev.* **103**, 1648 (1956).
- ¹⁰³ M. A. Lampert, *Rep. Prog. Phys.* **27**, 329 (1964).
- ¹⁰⁴ X. Zheng, B. Chen, J. Dai, Y. Fang, Y. Bai, Y. Lin, H. Wei, X. Zeng, and J. Huang, *Nat. Energy* **2**, 17102 (2017).
- ¹⁰⁵ Y. Yan, W. J. Yin, T. Shi, W. Meng, and C. Feng, in *Organic-Inorganic Halide Perovskite Photovoltaics: From Fundamentals to Device Architectures*, edited by N. G. Park, M. Grätzel, and T. Miyasaka (Springer International Publishing, Cham, 2016), p. 79.
- ¹⁰⁶ J. S. Park, S. Kim, Z. Xie, and A. Walsh, *Nat. Rev. Mater.* **3**, 194 (2018).
- ¹⁰⁷ W. J. Yin, T. Shi, and Y. Yan, *Appl. Phys. Lett.* **104**, 063903 (2014).
- ¹⁰⁸ A. Buin, P. Pietsch, J. Xu, O. Voznyy, A. H. Ip, R. Comin, and E. H. Sargent, *Nano Lett.* **14**, 6281 (2014).
- ¹⁰⁹ M. H. Du, *J. Phys. Chem. Lett.* **6**, 1461 (2015).
- ¹¹⁰ M. H. Du, *J. Mater. Chem. A* **2**, 9091 (2014).
- ¹¹¹ M. L. Agiorgousis, Y. Y. Sun, H. Zeng, and S. Zhang, *J. Am. Chem. Soc.* **136**, 14570 (2014).
- ¹¹² J. Kim, S. H. Lee, J. H. Lee, and K. H. Hong, *J. Phys. Chem. Lett.* **5**, 1312 (2014).
- ¹¹³ H. Shi and M. H. Du, *Phys. Rev. B* **90**, 174103 (2014).
- ¹¹⁴ F. De Angelis and A. Petrozza, *Nat. Mater.* **17**, 383 (2018).
- ¹¹⁵ D. Meggiolaro, S. G. Motti, E. Mosconi, A. J. Barker, J. Ball, C. Andrea Riccardo Perini, F. Deschler, A. Petrozza, and F. De Angelis, *Energy Environ. Sci.* **11**, 702 (2018).
- ¹¹⁶ D. Meggiolaro, E. Mosconi, and F. De Angelis, *ACS Energy Lett.* **2**, 2794 (2017).
- ¹¹⁷ D. Meggiolaro, E. Mosconi, and F. De Angelis, *ACS Energy Lett.* **3**, 447 (2018).
- ¹¹⁸ H. Uratani and K. Yamashita, *J. Phys. Chem. Lett.* **8**, 742 (2017).
- ¹¹⁹ A. Walsh and A. Zunger, *Nat. Mater.* **16**, 964 (2017).
- ¹²⁰ A. Zakutayev, C. M. Caskey, A. N. Fioretti, D. S. Ginley, J. Vidal, V. Stevanovic, E. Tea, and S. Lany, *J. Phys. Chem. Lett.* **5**, 1117 (2014).

- ¹²¹ R. E. Brandt, J. R. Poindexter, P. Gorai, R. C. Kurchin, R. L. Z. Hoye, L. Nienhaus, M. W. B. Wilson, J. A. Polizzotti, R. Sereika, R. Žaltauskas *et al.*, *Chem. Mater.* **29**, 4667 (2017).
- ¹²² Q. Wang, Y. C. Shao, H. P. Xie, L. Lyu, X. L. Liu, Y. L. Gao, and J. S. Huang, *Appl. Phys. Lett.* **105**, 163508 (2014).
- ¹²³ M. I. Saidaminov, J. Kim, A. Jain, R. Quintero-Bermudez, H. Tan, G. Long, F. Tan, A. Johnston, Y. Zhao, O. Voznyy *et al.*, *Nat. Energy* **3**, 648 (2018).
- ¹²⁴ Y. Tian, M. Peter, E. Unger, M. Abdellah, K. Zheng, T. Pullerits, A. Yartsev, V. Sundström, and I. G. Scheblykin, *Phys. Chem. Chem. Phys.* **17**, 24978 (2015).
- ¹²⁵ E. L. Unger, E. T. Hoke, C. D. Bailie, W. H. Nguyen, A. R. Bowring, T. Heumüller, M. G. Christoforo, and M. D. McGehee, *Energy Environ. Sci.* **7**, 3690 (2014).
- ¹²⁶ R. A. Belisle, W. H. Nguyen, A. R. Bowring, P. Calado, X. Li, S. J. C. Irvine, M. D. McGehee, P. R. F. Barnes, and B. C. O'Regan, *Energy Environ. Sci.* **10**, 192 (2017).
- ¹²⁷ P. Calado, A. M. Telford, D. Bryant, X. Li, J. Nelson, B. C. O'Regan, and P. R. F. Barnes, *Nat. Commun.* **7**, 13831 (2016).
- ¹²⁸ N. Aristidou, C. Eames, I. Sanchez-Molina, X. Bu, J. Kosco, M. S. Islam, and S. A. Haque, *Nat. Commun.* **8**, 15218 (2017).
- ¹²⁹ K. Huang and A. Rhys, *Proc. R. Soc. London, Ser. A* **204**, 406 (1950).
- ¹³⁰ H. Gummel and M. Lax, *Ann. Phys.* **2**, 28 (1957).
- ¹³¹ R. Kubo and Y. Toyozawa, *Prog. Theor. Phys.* **13**, 160 (1955).
- ¹³² B. K. Ridley, *Solid State Electron.* **21**, 1319 (1978).
- ¹³³ B. K. Ridley, *J. Phys. C: Solid State Phys.* **11**, 2323 (1978).
- ¹³⁴ T. Markvart, *J. Phys. C: Solid State Phys.* **14**, L895 (1981).
- ¹³⁵ C. H. Henry and D. V. Lang, *Phys. Rev. B* **15**, 989 (1977).
- ¹³⁶ T. Markvart, in *Recombination in Semiconductors*, edited by P. T. Landsberg (Cambridge University Press, Cambridge, 2003), p. 474.
- ¹³⁷ A. Alkauskas, M. D. McCluskey, and C. G. Van de Walle, *J. Appl. Phys.* **119**, 181101 (2016).
- ¹³⁸ B. K. Ridley, *Quantum Processes in Semiconductors* (Oxford University Press, Oxford, 2013), p. 186.
- ¹³⁹ T. Kirchartz, T. Markvart, U. Rau, and D. A. Egger, *J. Phys. Chem. Lett.* **9**, 939 (2018).
- ¹⁴⁰ T. Markvart, in *Recombination in Semiconductors*, edited by P. T. Landsberg (Cambridge University Press, Cambridge, 2003), p. 467.
- ¹⁴¹ B. K. Ridley, *Quantum Processes in Semiconductors* (Oxford University Press, Oxford, 2013), p. 224.
- ¹⁴² D. K. Ferry, *Semiconductors: Bonds and Bands* (IOP Publishing, Bristol, UK, 2013).
- ¹⁴³ M. Sendner, P. K. Nayak, D. A. Egger, S. Beck, C. Müller, B. Epding, W. Kowalsky, L. Kronik, H. J. Snaith, A. Pucci *et al.*, *Mater. Horiz.* **3**, 613 (2016).
- ¹⁴⁴ Y. Shao, Y. Yuan, and J. Huang, *Nat. Energy* **1**, 15001 (2016).
- ¹⁴⁵ D. Luo, W. Yang, Z. Wang, A. Sadhanala, Q. Hu, R. Su, R. Shivanna, G. F. Trindade, J. F. Watts, Z. Xu *et al.*, *Science* **360**, 1442 (2018).
- ¹⁴⁶ Y. Hou, X. Du, S. Scheiner, D. P. McMeekin, Z. Wang, N. Li, M. S. Killian, H. Chen, M. Richter, I. Levchuk *et al.*, *Science* **358**, 1192 (2017).
- ¹⁴⁷ H. Tan, A. Jain, O. Voznyy, X. Lan, F. P. Garcia de Arquer, J. Z. Fan, R. Quintero-Bermudez, M. Yuan, B. Zhang, Y. Zhao *et al.*, *Science* **355**, 722 (2017).
- ¹⁴⁸ S. S. Shin, E. J. Yeom, W. S. Yang, S. Hur, M. G. Kim, J. Im, J. Seo, J. H. Noh, and S. I. Seok, *Science* **356**, 167 (2017).
- ¹⁴⁹ N. Arora, M. I. Dar, A. Hinderhofer, N. Pellet, F. Schreiber, S. M. Zakeeruddin, and M. Grätzel, *Science* **358**, 768 (2017).
- ¹⁵⁰ R. Brendel and R. Peibst, *IEEE J. Photovoltaics* **6**, 1413 (2016).
- ¹⁵¹ C. Katan, A. D. Mohite, and J. Even, *Nat. Mater.* **17**, 377 (2018).
- ¹⁵² J. Even, M. Carignano, and C. Katan, *Nanoscale* **8**, 6222 (2016).
- ¹⁵³ O. Yaffe, Y. Guo, L. Z. Tan, D. A. Egger, T. Hull, C. C. Stoumpos, F. Zheng, T. F. Heinz, L. Kronik, M. G. Kanatzidis *et al.*, *Phys. Rev. Lett.* **118**, 136001 (2017).
- ¹⁵⁴ A. Baumann, S. Vöth, P. Rieder, M. C. Heiber, K. Tvingstedt, and V. Dyakonov, *J. Phys. Chem. Lett.* **6**, 2350 (2015).
- ¹⁵⁵ G. Landi, H. C. Neitzert, C. Barone, C. Mauro, F. Lang, S. Albrecht, B. Rech, and S. Pagano, *Adv. Sci.* **4**, 1700183 (2017).
- ¹⁵⁶ A. Poglitsch and D. Weber, *J. Chem. Phys.* **87**, 6373 (1987).
- ¹⁵⁷ T. Markvart, in *Recombination in Semiconductors*, edited by P. T. Landsberg (Cambridge University Press, Cambridge, 2003), p. 475.
- ¹⁵⁸ J. Heyd, G. E. Scuseria, and M. Ernzerhof, *J. Chem. Phys.* **118**, 8207 (2003).